The Thesis Committee for Greg John Dahlberg
Certifies that this is the approved version of the following thesis:

Fault Clearance in Distributed Power Architectures with Limited Energy Flow through Power Electronic Interfaces

APPROVED BY
SUPERVISING COMMITTEE:

Supervisor:

Alexis Kwasinski

William Mack Grady

Fault Clearance in Distributed Power Architectures with Limited Energy Flow through Power Electronic Interfaces

by

Greg John Dahlberg, M.Ed., B.S.

Thesis

Presented to the Faculty of the Graduate School of

The University of Texas at Austin

in Partial Fulfillment

of the Requirements

for the Degree of

Master of Science in Engineering

The University of Texas at Austin

May 2012

Dedication

Dedicated to my beautiful wife Sarah, to my handsome son Logan, and to the one on the way.

Acknowledgements

I would like to thank Dr. Alexis Kwasinski for his help and guidance on this thesis. It was through his teachings that I was introduced to the concepts of micro-grids and distributed generation. I would like to thank my thesis reader and teacher, Dr. Mack Grady. I would also like to thank the gentlemen of the Power Electronics Group at the University of Texas for all the help in constructing and performing physical experiments. Finally, I would like to thank my wife for having the patience to proof read my thesis.

Abstract

Fault Clearance in Distributed Power Architectures with Limited Energy Flow through Power Electronic Interfaces

Greg John Dahlberg, M.S.E.

The University of Texas at Austin, 2012

Supervisor: Alexis Kwasinski

The objective of this thesis is to determine a method for computing the amount of capacitance in a power electronic converter required to melt a fuse in the event of a line to ground fault. DC micro-grids rely on power electronic converters to change voltage levels. All converters rely on semiconductor switches that must be protected from surges of fault current. This limits the power that a converter can supply to a fuse. In many cases, sufficient power may be achieved by appropriately sizing the converters' output capacitor.

Table of Contents

List of Tables

List of Figures

Chapter 1: Introduction

One of the great inventions of the late nineteenth century was the AC electric voltage transformer. This development helped usher in the age of AC power transmission, subsequently "defeating" Edison's DC power [1] [2] [3]. The ability to transmit power by increasing voltage and decreasing current translated to a substantial decrease in ohmic power losses and an increase in power efficiency. This allowed for the efficient transfer of electric power over great distances which catalyzed the era of large centralized power plants [1]. Currently, conventional large-scale steam power plants produce over 85% of the electricity in the United States [4] from remote locations. Large-scale natural gas and hydro generation plants produce the other 15% [4].

There are three ongoing developments that began toward the end of the twentieth century that could bring about a new era in energy generation, with DC power generation a sizable portion of the energy portfolio. The first innovation was the development of power electronic converters. Since the invention of solid state switches in the fifties, the field of DC/DC and DC/AC converters has grown rapidly [5]. This allows for the easy manipulation of DC voltages that did not exist in the days of Edison and Tesla. With DC/DC converters, a DC voltage can be increased to limit the distribution current and allow for efficient transfer of DC power.

The second development is the desire for renewable forms of energy production [1]. A majority of climate scientists maintain that the Earth's temperature is steadily increasing due in part to the burning of fossil fuels [6] [7]. There is also great concern over the dwindling supply of fossil fuels [8]. These concerns among others have motivated research into the production of environmentally clean electricity [1] [9]. This includes photovoltaics, fuel cells, wind turbines and storage batteries [9]. All of these,

except wind turbines, produce a DC voltage. In the case of wind turbines, they must first be rectified and then inverted to match the 60 hertz frequency of the US electric grid [10]. In a pure DC grid, the AC inversion stage for wind turbines can be omitted and any conversion stage for DC power producers can likewise be omitted [3].

The third major development that promotes the feasibility of DC grids is the rapid increase in electronic loads [11] [3]. Computers, laptops, television sets, fluorescent lights and cell phone chargers are a few of the many common household electronic loads that require rectification to DC [3]. Other load types such as resistive heating elements and motors can also be operated with DC power [3]. A DC grid will circumvent the rectification conversion stage which has the effect of increasing efficiency, lowering capital costs and increasing overall energy availability [10] [3].

However, a dramatic change from an AC grid to a DC grid would likely be very expensive and pose many logistical and political problems. One solution to this is the development of a so-called micro-grid [10] [11] [3] [12]. A micro-grid can be loosely defined as a collection of distributed power generating units, a collection of loads served by these units and a distribution grid [10] [11] [3] [12]. It is typically interfaced with the main grid, but may disconnect from the grid during upstream faults. During a disconnected “islanded mode”, dedicated generators will ideally continue to supply loads in the micro-grid with uninterrupted power [10] [11] [3] [12]. This has the effect of increasing the energy availability to the loads it serves [13] [10]. While there has been some research conducted on pure DC micro-grids, a lot of research is focused on hybrid micro-grids that have sections of both AC and DC power [14] [15] [16] [17]. This is a consequence of the fact that not all loads can be operated with DC power. Since micro-grids harbor small micro-turbines located close to their loads, the initial capital cost of implementing them will be small, relative to the more expensive option of creating

remote large-scale power plants [10] [3]. From a capital cost perspective, the modularity of small generation units makes them an attractive investment. Distributed generation is therefore a practical means for making renewable forms of energy production competitive with conventional power plants.

Increased efficiency and energy availability along with integration of renewables are just a few of the benefits researchers claim that micro-grids offer [10] [18] [3]. While an abundance of research to date has articulated the numerous virtues of DC micro-grids, there are many remaining issues. A lot of the current research is focused on these problems.

One major concern is the protection of micro-grids against faults [11] [3] [19] [20] [21] [22] [23]. In low voltage settings, fuses are typically used to protect equipment against faults [10] [24] [11] [3]. DC micro-grids rely on power electronic converters to adjust voltage levels [10] [11] [3]. The existence of relatively low current rated MOSFET or IGBT switches in power converters creates the need for current limitation through the power electronic device [10] [25]. Limited current flow translates to limited power flow. In the case of a downstream fault, this limited power flow may prove to be insufficient to heat and melt a protective fuse [10] [25]. As a result, the affected load and other feeders connected to the converter will see a current surge which can destroy any electronic device plugged into the distribution grid.

Figure 1.1 illustrates the general system studied. A DC voltage feeds a power converter which sets the output capacitor voltage level. The controller modulates the output voltage via a P.I control scheme. The controller further regulates the inductor current to values less than a set maximum,$i_{L,max}$. If R_1experiences a fault then the fuse which connects it to the distribution grid needs to open to prevent the fault from propagating through R_2. R_2 may be the equivalent resistance for n parallel loads. The

current seen by the fuse during steady state operation can be computed as the ratio of capacitor voltage to equivalent parallel resistance of all n+1 resistive elements. For this reason the R_2 leg need not be considered if R_1 is replaced by an equivalent resistance.

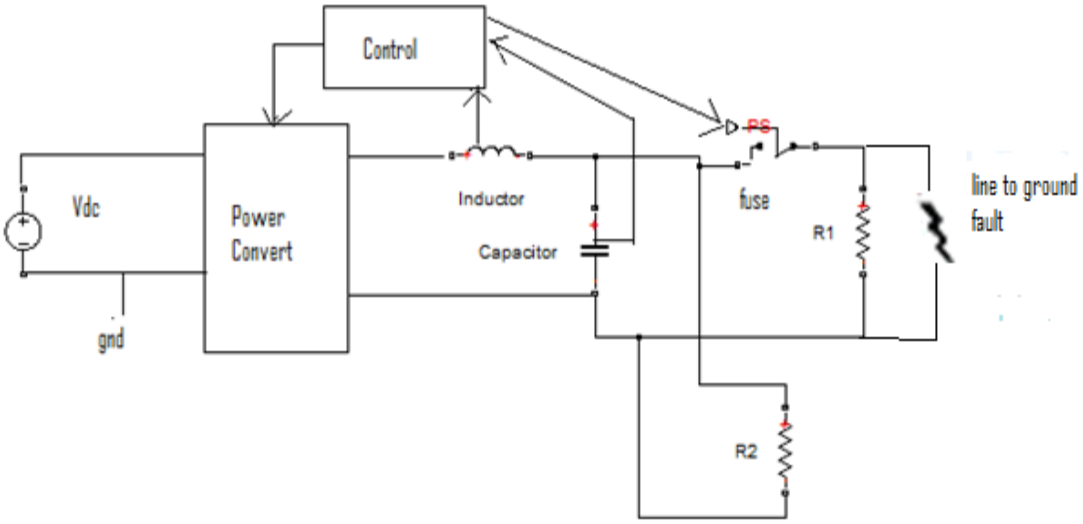

Figure 1.1: General Circuit Topology

There have been many strategies proposed to protect DC micro-grids [3] [19] [20] [21] [22] [23] but few seem to address the problem of limited power flow. One solution is to add energy storage elements such as batteries to supplement the fault current to melt the fuse [26]. Another solution is to increase the capacitance in the output capacitor of the low pass filter in the power device [10] [25]. When a downstream fault occurs, the inductor current rapidly increases to the maximum value allowed by the current limiter. At roughly the same time, the output capacitor discharges its stored energy creating a current spike through the capacitor. The inductor's and capacitor's currents sum constructively to give the fault current as shown in Figure 1.2. After a short period of time, the fault current decreases to the level of the maximum inductor current.

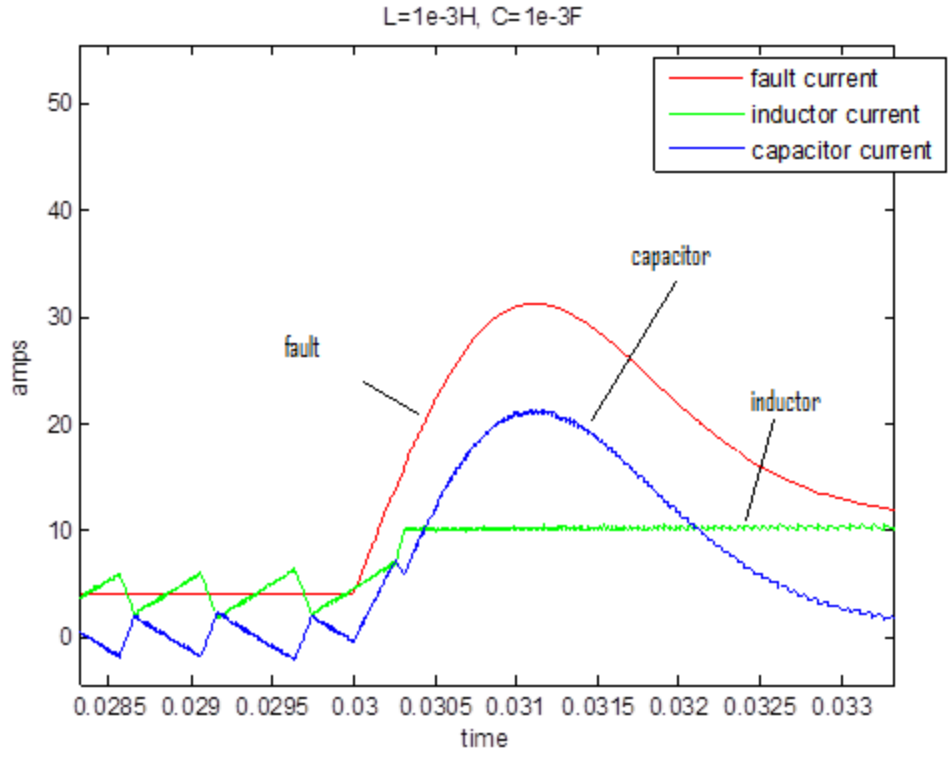

Figure 1.2: Output Currents

This phenomenon can be algebraically expressed as:

$$i_L + i_C = i_f \tag{1.1}$$

Increasing the capacitance results in an increase in capacitor current according to the equation:

$$i_c = -C\frac{dv_c}{dt} \tag{1.2}$$

Therefore, by properly sizing the output capacitor, sufficient energy proportional to $\int i_f^2 dt$, can be delivered to the fuse, melting it before the fault current propagates to the connected load and any additional feeders.

There has been numerous studies conducted regarding protection implementation schemes for DC micro-grids [3] [19] [20] [21] [22] [23]. This research is often concerned with the detection and isolation of faults via complex control schemes. Papers like [21] and [27] focus on fault protections via overcurrent relay protection models. Often the research is specialized to different types of electrical faults such as series or parallel. In [28], for instance, series faults are studied and the generated DC arcs are compared with AC arcs. However, there has been less research on the effects of capacitors' and other types of energy storage devices' abilities to clear a fault by providing sufficient energy to melt a fuse. Some exceptions are found in [10] [11] [25] [12]. Papers such as [10] and [11] propose that sufficient energy can be realized by appropriately sizing the output capacitor of the power converter. A closed form solution that expresses the minimum amount of capacitance required to clear a fuse can be found in [10]. This solution is written in terms of the fuse parameters and the current and voltage characteristics of the system. While [10] gives a very simple equation for computing the amount of energy a capacitor can deliver to a fuse, it neglects the current in the inductor which supplements the energy in the capacitor.

This thesis is focused on determining a method for computing the amount of capacitance required to clear a fuse in the event of a parallel fault based on the published I^2t value when the system's power flow is limited. According to [29], the published I^2t value is a good measure of the aggregate overcurrent of energy that a fuse can sustain before opening. Chapter 2 will give an overview of the methodology involved. In Chapter 3, a closed form solution for the fault current is derived. Chapter 4 is concerned with a correction to the general fault current equation derived in Chapter 3. Chapter 5 gives a circuit theory argument that a parallel fault can be modeled as an equivalent time dependent impedance. Chapter 6 explains the experimental tests that were conducted to

empirically determine the validity of the theory presented here. In Chapter 7, an alternate method for computing capacitance will be presented. In this method a closed form solution for capacitance will be derived and theoretical results will be compared with simulation results. This thesis is then concluded in Chapter 8.

Chapter 2: Fault Current Derivation

2.1 Methodology

The first objective of this project is to develop a simple analytic expression for the fault current as a function of the systems parameters. Fuse manufacturing companies should publish an I^2t number that is proportional to the amount of energy required to melt the fuse. Also required is knowledge of the maximum current through the fuse before the fuse begins to melt. Once this is known, the time at which the fault current exceeds the maximum current rating and the time at which the fault current returns to the maximum current rating can be numerically computed. The square of the fault current can then be integrated with respect to time between the appropriate roots of equation (2.1). If this definite integral is greater than the published I^2t rating, then it is expected that sufficient heat energy will be transferred to melt the fuse, clearing the fault. If the upper root of equation (2.1) is large, allowing some fault current to propagate before the fuse is cleared, then the upper limit of (2.2) can be set to an earlier time. For a given amount of output capacitance C, t_e in (2.2) is the amount of time required to clear the fault, thereby satisfying the equation $f(t_e) = 0$.

$$i_f(t) = i_{L,max} \tag{2.1}$$

$$f(t_e) = \int_{t_s}^{t_e} i_f^2 \, dt - I^2t \tag{2.2}$$

Where $i_f(t_e) = i_{L,max}$ and $i_f(t_s) \approx i_{L,max}$

2.2 Modeling Parallel Faults

In a parallel fault, defined here as a short circuit parallel with the output capacitor, the voltage drop across the shorted capacitor should decrease as an inverse exponential [4]. This is equivalent to a resistor in parallel with the load decreasing at a rapid negative exponential rate. For small time constants, it is proposed here that the inverse time function:

$$R_f = \frac{a}{t\prime - t_f} \equiv \frac{a}{t} \tag{2.3}$$

can be used to model the short circuit. This is preferable to using the negative exponential function since the negative exponential leads to a much more difficult integral in the solution. The a parameter determines the rate of decrease and, from equation (2.3), it is seen that t_f can be chosen so as to determine the initial resistance at the time of the fault. The domain of t is the time of the fault to positive infinity. The t_f parameter should be chosen close to the time of the fault and prior to the fault since negative resistances will otherwise result. From Figure 1.1 it is seen that the equivalent resistance equals the load resistance R_L in parallel with the fault resistance R_f which can be expressed as:

$$R \equiv R_{equiv} = \frac{R_L * R_f}{R_L + R_f} = \frac{a * R_L}{R_L * t + a} \tag{2.4}$$

2.3 Fundamental Equations

Since the capacitor and equivalent resistance are in parallel, as seen in Figure 1.1, the voltage across the capacitor will equal the voltage across the resistance.

$$V_c = V_R \tag{2.5}$$

The voltage across the resistance can be expressed in terms of the fault current as

$$V_R = i_f * R \tag{2.6}$$

Here R is the equivalent resistance given in equation (2.4). The capacitor voltage is therefore

$$V_c = i_f * R \tag{2.7}$$

2.4 General Fault Current Derivation

Taking the time derivative of (2.7) and multiplying by the capacitance $-C$ gives the capacitor current in accordance with (2.8).

$$i_c = -C\dot{V}_c = -C * \left(\dot{i}_f R + i_f \dot{R}\right) \tag{2.8}$$

This can be substituted into (1.1) yielding the linear first order non-homogenous differential equation:

$$\frac{di_f}{dt} + i_f \left(\frac{C*\frac{dR}{dt}-1}{CR}\right) = \frac{i_L}{CR} \tag{2.9}$$

This differential equation has the solution:

$$i_f = \exp\{-\int P(t)dt\} * \int\{Q(t) * \exp\{\int P(t)dt\} + K\}dt \qquad (2.10)$$

Where K is a constant and

$$P = \frac{C*\frac{dR}{dt}-1}{CR} \qquad (2.11)$$

$$Q = \frac{i_L}{CR} \qquad (2.12)$$

2.5 Inductor Current Approximation

A problem with equation (2.10) is that the inductor current i_L is unknown. Figure 2.1 suggests that the average inductor current can be approximated by three piecewise defined functions.

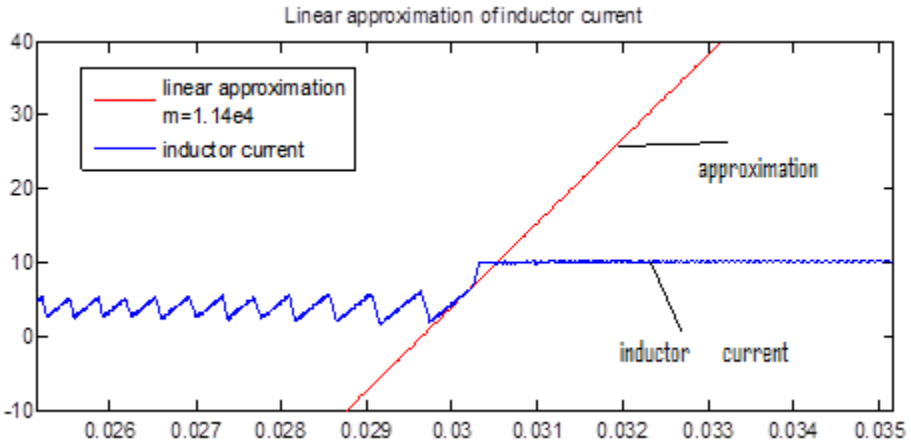

Figure 2.1: Inductor Current Approximation

$$i_L(t) = \begin{cases} \frac{V_C}{R_L}; & t \le t_f \\ m(t - t_f) + i_{L,steady\ state}; & t_f \le t \le t_f + (i_{L,max} - i_{L,ss})/m \\ i_{L,max}; & t \ge t_f + (i_{L,max} - i_{L,ss})/m \end{cases} \quad (2.13)$$

In (2.13) m is the slope of the inductor current, $i_{L,max}$ is the maximum current allowed by the current regulator and $i_{L,ss}$ is the average steady state current given by:

$$i_{L,ss} = \frac{V_C}{R_L}; \quad t \le t_f \quad (2.14)$$

Since m is very large and the inductor increases linearly for a very brief period, the inductor current can be approximated as:

$$i_L(t) = \begin{cases} \frac{V_C}{R}; & t \le t_f \\ i_{L,max}; & t > t_f \end{cases} \quad (2.15)$$

The additive constant K should be determined by computing (2.10) at the time of the fault and setting this value equal to the inductor steady state current $i_{L,ss}$.

Simulations show that this approximation will introduce a significant error in the computation of the fault current. A technique to minimize this error will be given in chapter 4.

2.6 Fault Current

Since the inductor current is now assumed to be constant and at its maximum value from the time of the fault, it can be pulled out of the integral leading to the solution [30]:

$$i_f = (R_L t + a)\, exp\big(-(\alpha_1 t^2 + \alpha_2 t)\big) * \{\frac{i_{L,max}}{2aCR_L}\sqrt{\frac{\pi}{\alpha_1}}\exp\left(\frac{-\alpha_2^2}{4\alpha_1}\right) * erfi\left(\left(\sqrt{\alpha_1}t + \frac{\alpha_2}{2\sqrt{\alpha_1}}\right) * j\right)/j + K\} \quad (2.16)$$

K, α_1 and $\alpha_2$are constants given by:

$$K = i_{L,ss} * \frac{\exp\left(\alpha_1 t_f^2 + \alpha_2 t_f\right)}{R_L t_f + a} - \frac{i_{L,ss}}{2CaR_L}\sqrt{\frac{\pi}{\alpha_1}}\exp\left(\frac{-\alpha_2^2}{4\alpha_1}\right) erfi(\left(\sqrt{\alpha_1}t_f + \frac{\alpha_2}{2\sqrt{\alpha_1}}\right)j)/j \quad (2.17)$$

$$\alpha_1 = \frac{1}{2aC},\ \alpha_2 = \frac{1}{CR_L}$$

In (2.16) and (2.17) $erfi(zj)$ is the imaginary error function often found in probability theory. It is related to the real error function by

$$erfi(z) = -jerf(zj) = -j\sqrt{\frac{2}{\pi}}\int_0^{jz} e^{-t^2} dt \quad (2.18)$$

Equation (2.16) gives the fault current for the graph in Figure 1. (Any parallel loads should first be reduced to an equivalent single load which will increase the initial steady state inductor current.) Interestingly, the term $\exp\big(-(\alpha_1 t^2 + \alpha_2 t)\big)$ approaches zero very rapidly while $erfi\left(\left(\sqrt{\alpha_1}t + \frac{\alpha_2}{2\sqrt{\alpha_1}}\right) * j\right)/j$ approaches infinity very rapidly as seen in Figure 2.2. The product of these terms, along with $\big(R_1 t_f + a\big)$, will tend to a positive constant proportional to $i_{L,max}$ after a short amount of time.

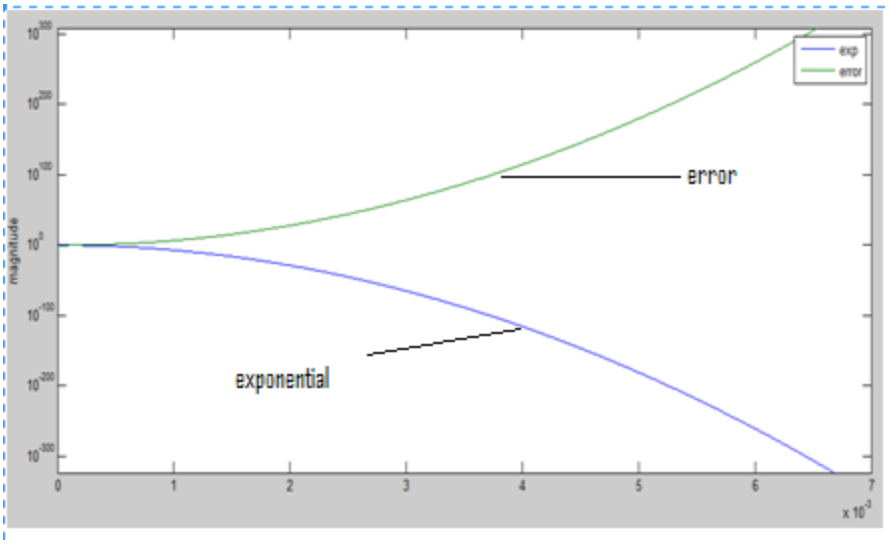

Figure 2.2: Divergence of Fault Current Terms

Multiplying two rapidly divergent terms has the unfortunate consequence that i_f will be highly sensitive to certain parameters. In particular, in order to compute the constant K, $i_f(t_f)$ must be computed. However K is very sensitive to the choice of t_f. Chapter 4 attempts to deal with this problem by determining how t_f varies with inductance and capacitance.

The squared time integral whose endpoints are the roots of equation (2.1) can now be numerically computed. If this integral is greater than the given I^2t value of the fuse, then the capacitor is large enough to clear the fault. Let E be the fuse's I^2t value and consider the slight variation to equation (2.2):

$$h(t_e, C) = \int_{t_f}^{t_e} i_f(t', C)^2 dt' - E \tag{2.19}$$

The minimum sufficient capacitance can be calculated by determining the roots of (2.19). It should be obvious that the correct physical solution to (2.19) will also satisfy the condition: $\frac{dh(t_e,C)}{dC} > 0$.

This highly nonlinear problem can be solved by either using numerical techniques such as the Newton Raphson method or, since the problem is relatively small, a simple programming loop can be used to find the amount of capacitance that brings (2.19) sufficiently close to zero.

Chapter 3: t_0 Correction

3.1 t_0 Parameter

Using equation (2.15) for the inductor current rather than equation (2.13) results in an overestimate of the fault current. An alternative inductor function is given in (3.1)

$$i_L(t) = \begin{cases} \frac{V_C}{R}; & t \leq t_0 \\ - & \\ i_{L,max}; & t > t_0 \end{cases} \tag{3.1}$$

Note that t_0 is used rather than t_f. This idea uses the basic result from elementary calculus that the area under the graph of an increasing function f in the interval [a,b] is equal to the maximum value of f times some number t_0 in the interval [a,b]. Figure 3.1 illustrates this concept.

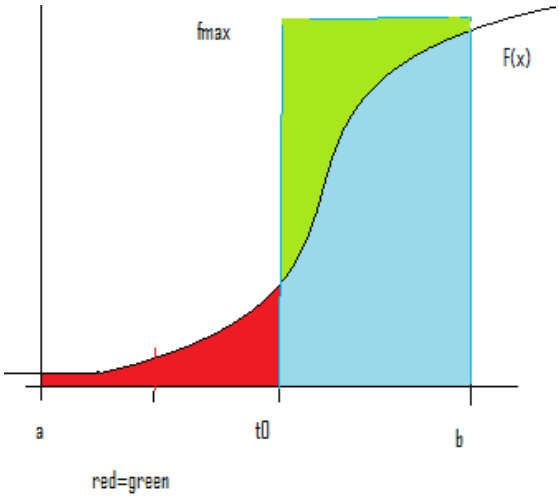

Figure 3.1: t_0 Correction

From Figure 3.1 it is seen that there exists a $t_0 \in [a, b]$ such that $\int_a^b f(x)dx = f(b) * (b - t_0)$. Graphically, t_0 can be varied until the green area equals the red area. To find the value t_0, the difference in the maximums between the simulation current $i_{f,sim}$ and the fault current equation $i_{f,equat}$ is minimized over t_0 in the interval [a,b]. That is, the optimization problem (3.2) is solved.

$$min_{t_0 \in [a.b]} \ |\max(i_{f,sim}) - \max(i_{f,equat})| \tag{3.2}$$

3.2 Fault Current Approximation Improvement

The results of this technique give a very accurate analytic solution as expressed in (2.16). The difference between the uncorrected fault current solution with the simulation and corrected fault current solution with the simulation are shown in Figures 3.2 and 3.3 respectively. The red graphs are the Simscape™ generated graphs and the blue graphs are the graphs computed using (2.16) along with the correction (3.2).

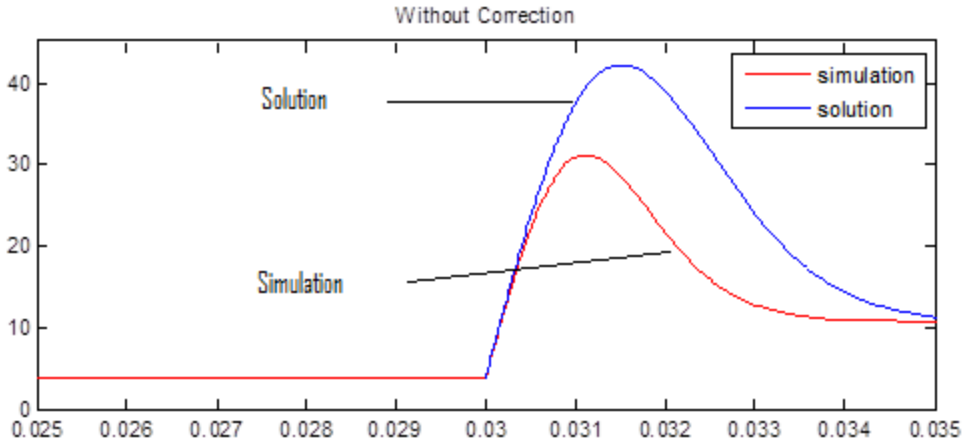

Figure 3.2: Uncorrected Fault Current

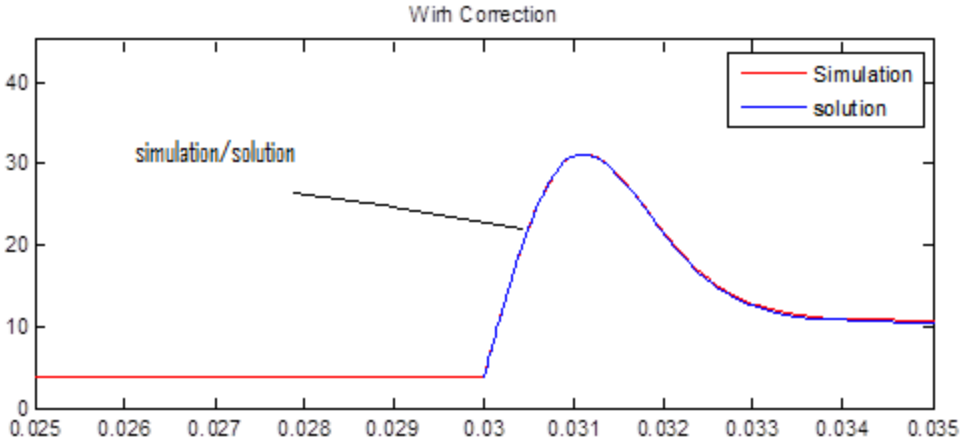

Figure 3.3: Corrected Fault Current

As can be seen from Figure 3.3, the solution graph is almost exactly the same as the simulation graph after the fault occurs. However, it would be preferable to have an analytic expression for the fault current that does not depend on solving (3.2) for t_0. A solution that is independent of simulation is desirable so that engineers applying this technique will not have to construct the Simscape™ model, run simulations, collect data and then write programs to solve the equations. The task would be simplified to solving the equations.

Toward this end, the dependence of t_0 on capacitance and inductance was studied. Figure 3.4 shows how $t_0$varies as capacitance increases for various values of inductance which are given in the legend. All graphs within a certain domain of capacitance approximately decrease as the inverse of capacitance.

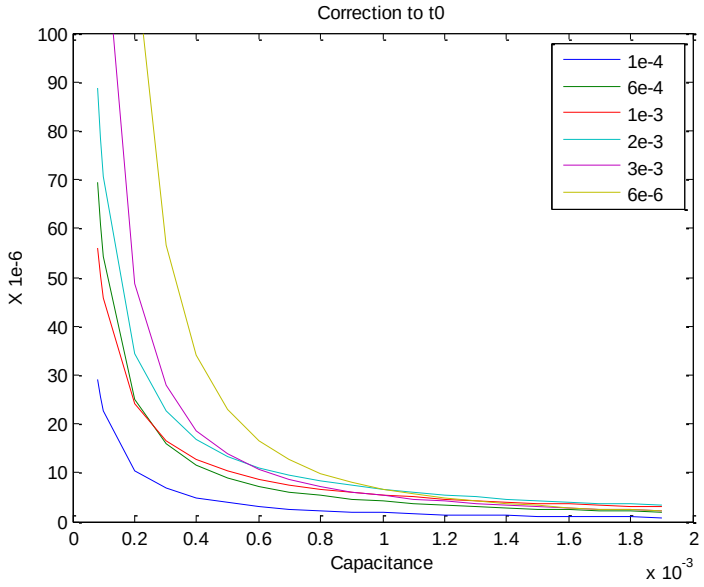

Figure 3.4: Variation of t0 with Capacitance

This variation with inverse capacitance breaks down for larger inductances:

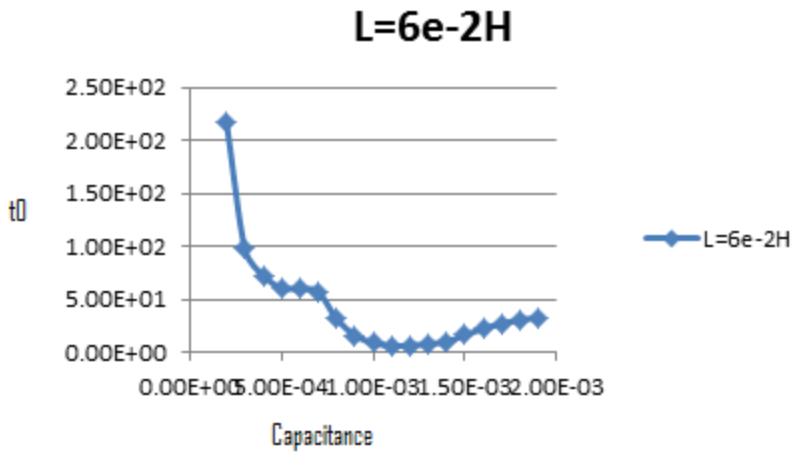

Figure 3.5: Relation Breakdown

3.3 t_0 Parameterization

Figure 3.4 motivates the following relation between t_0 and C:

$$t_0 = \frac{a}{C^b} \tag{3.3}$$

a and b are parameters to be determined

For inductance equal to L=6e-4 H equation (3.3) was curve fit using Microsoft® Excel. This is shown in Figure 3.6.

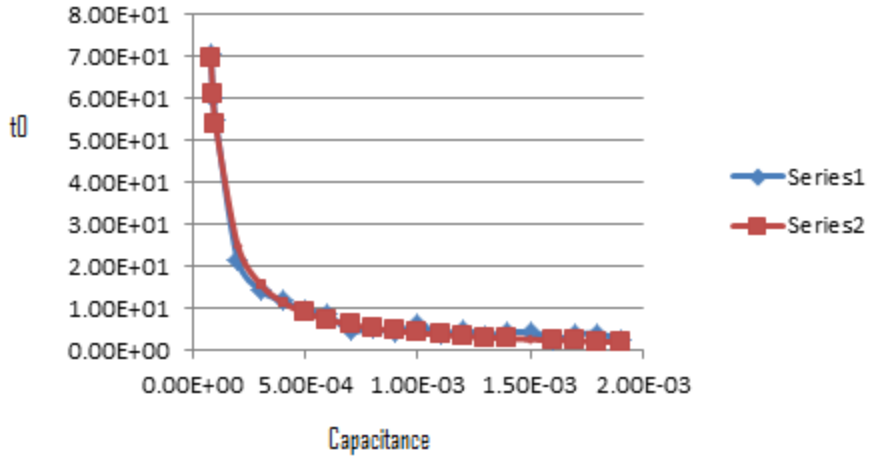

Figure 3.6: Excel Curve Fit for t0

This process was repeated for six values of inductance, ranging from 1e-4 H to 6e-3 H. The a and b values were calculated for each case. These calculated values were then taken and plotted against inductance. The graphs of a versus L and b versus L are given in Figure 3.7 and 4.8, respectively.

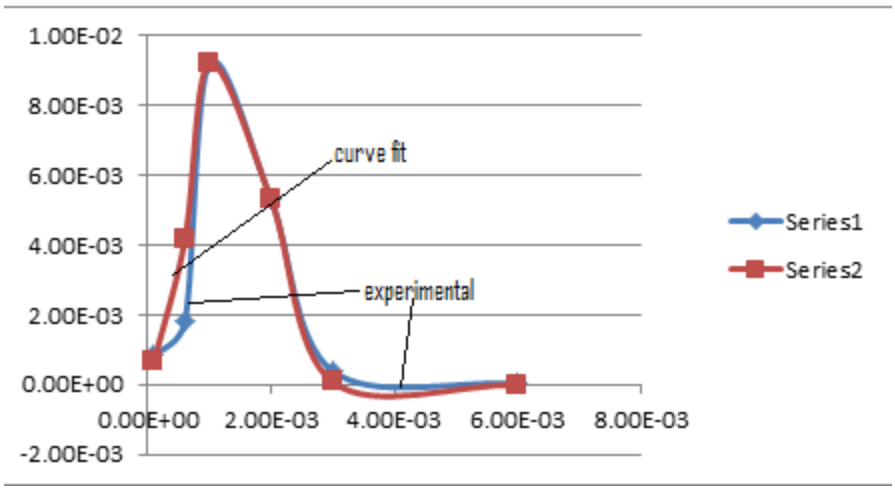

Figure 3.7: ‘a’ Parameter Variation

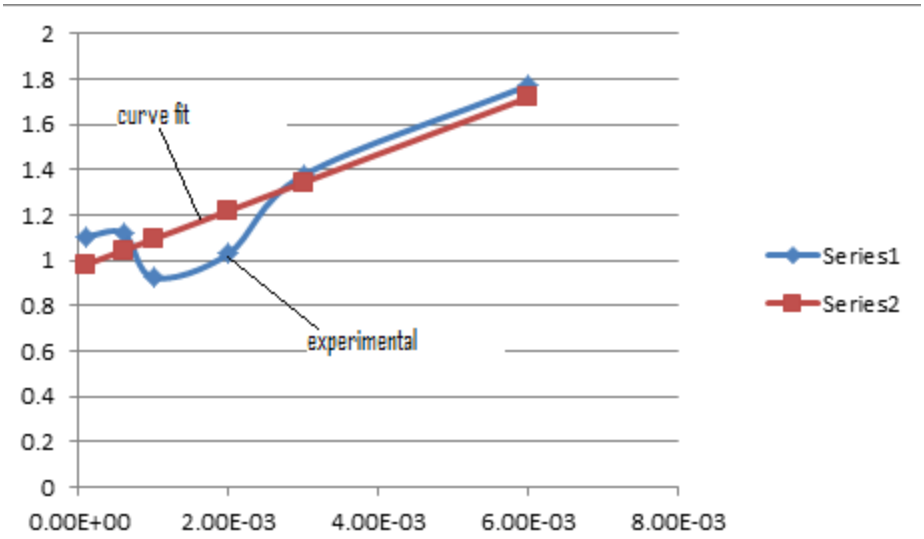

Figure 3.8: 'b' Parameter Variation

These curves were then approximated and fit using Microsoft® Excel solver. The red curves in figures 4.7 and 4.8 are the approximate curve while blue curves are the experimental curves. Equations (3.4) and (3.5) give closed form approximations for a and b respectively. Using these equations and equation (3.2) gives an expression for t_0:

$$a = 4.22e-10 * exp(-1816577.97965541 * L\text{^}2 + 4899.62979024404 * L) \quad (3.4)$$

$$b = 124.7669 * L + .97014 \quad (3.5)$$

$$t_0 = \frac{4.22e-10*exp(-1816577.97965541*L\text{^}2+4899.62979024404*L)}{C^{124.7669*L+.97014}} \quad (3.6)$$

3.4 I^2t values

The simulation fault current and analytic fault current with t_0 correction for L=1e-4 and C=3e-3 are given in Figure 3.9.

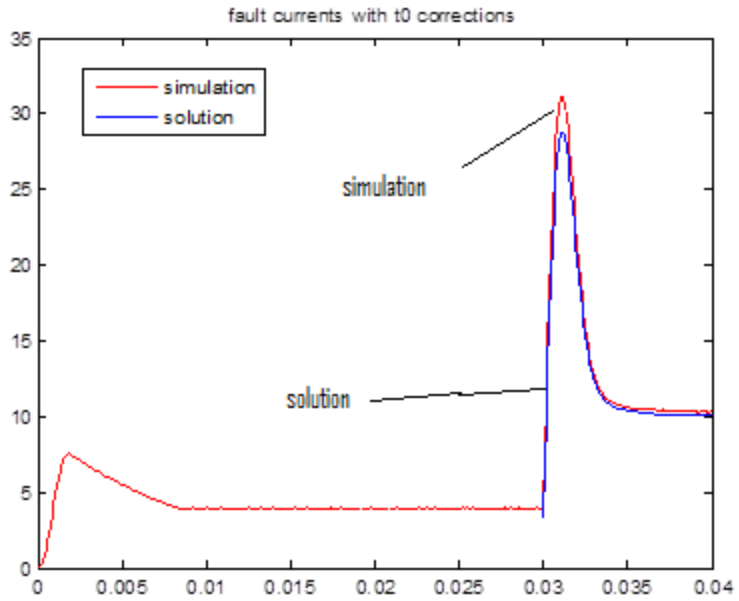

Figure 3.9: Fault Current with t0 Variation

As the graph illustrates, this is a reasonable match and the solution is less than the simulation, making an underestimate of capacitance less likely. Next, the ratio of simulation I^2t values and solution I^2t values was computed for various values of inductance and capacitance. Some results are tabulated in Table 3.1.

		L					
i^2 error		1.00E-04	6.00E-04	1.00E-03	2.00E-03	3.00E-03	6.00E-03
C	8.00E-05	0.709625					1.06E+00
	9.00E-05						
	1.00E-04					1.017718	
	2.00E-04					1.0288	
	3.00E-04						
	4.00E-04					1.035784	
	5.00E-04			0.887475			
	6.00E-04						
	7.00E-04						
	8.00E-04						
	9.00E-04					1.043898	
	1.00E-03		0.973079		0.883644		
	1.10E-03		0.959263				1.099502
	1.20E-03		0.980197				
	1.30E-03		0.97789				
	1.40E-03						
	1.50E-03						
	1.60E-03				0.903111		
	1.70E-03						
	1.80E-03						
	1.90E-03	0.945622		0.92889			1.11E+00

Table 3.1: Relative I^2t Values for Large 'a' Values

Values in Table 3.1 less than one indicate that equation (2.16) is an underestimate while values greater than one indicate an overestimate. As can be seen by the few calculated values, most are within 5% of unity while only a couple are at 10%. It is expected, though not proven, that the more reasonable the values of inductance and capacitance are for a given system, the closer the ratios in Table 3.1 will be to unity.

This analysis breaks down for $a < 10^{-4}$. Analysis from the next chapter will show that it is necessary to have values that work below this limit and down to the level of $a = 10^{-7}$. The same procedure of running simulations in Simscape™, recording the

data in Microsoft® Excel and analyzing the data in MATLAB® was carried out to determine how t_0 depends on inductance and capacitance. Figure 3.10 shows this dependence.

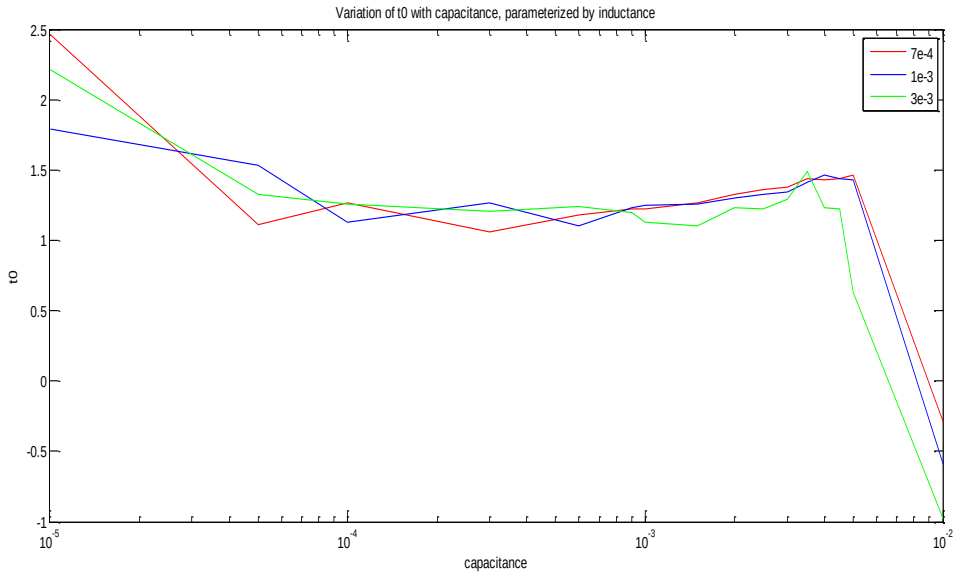

Figure 3.10: Variation of t0 with Capacitance

For values of capacitance in the range $3 * 10^{-4} < C < 5 * 10^{-3}$ the approximation $t_0 = 1.25 * 10^{-8}$ works very well. Table 3.2 gives the ratio of the theoretical computation of the I^2t value to the simulation value. As before, numbers less than one indicate that the theoretical calculation is an underestimate of the total "let through" energy. A slight underestimate is preferable to an overestimate since it leads to slight oversizing of the capacitor which will ensure that the fuse melts.

Cap\ Inductance	1.00E-04	7.00E-04	1.00E-03	3.00E-03
1.00E-05	5.00E-02	0.060821	0.06421	0.095484
5.00E-05	3.29E-01	0.378966	0.396867	0.500534
1.00E-04	5.57E-01	0.626391	0.621963	0.725184
3.00E-04	7.77E-01	0.853316	0.888918	0.90784
6.00E-04	8.85E-01	0.926071	0.916632	0.951245
9.00E-04	9.24E-01	0.94803	0.949973	0.957726
1.00E-03	9.33E-01	0.948422	0.958696	0.94408
1.50E-03	9.47E-01	0.961247	0.962865	0.9398
2.00E-03	9.40E-01	0.9746	0.969803	0.963723
2.50E-03	9.60E-01	0.977061	0.975697	0.961735
3.00E-03	9.57E-01	0.981951	0.973897	0.972864
3.50E-03	9.63E-01	0.99124	0.98648	1.001873
4.00E-03	9.73E-01	0.985874	0.993959	0.95608
4.50E-03	9.77E-01	0.986144	0.986885	0.955788
5.00E-03	9.77E-01	0.988663	0.985967	8.57E-01
1.00E-02	9.82E-01	0.705197	0.662275	0.6108

Table 3.2: Relative I^2t Values for small 'a' Values

The red numbers indicate good approximations. Simulation shows that $t_0 = 1.25 * 10^{-8}$ works well for a wider range of inductive values that are tabulated here.

3.5 Plot I^2t Against Capacitance

With the fault current known, the I^2t values can be calculated and plotted against capacitance. A linear relation is observed from Figure 3.11.

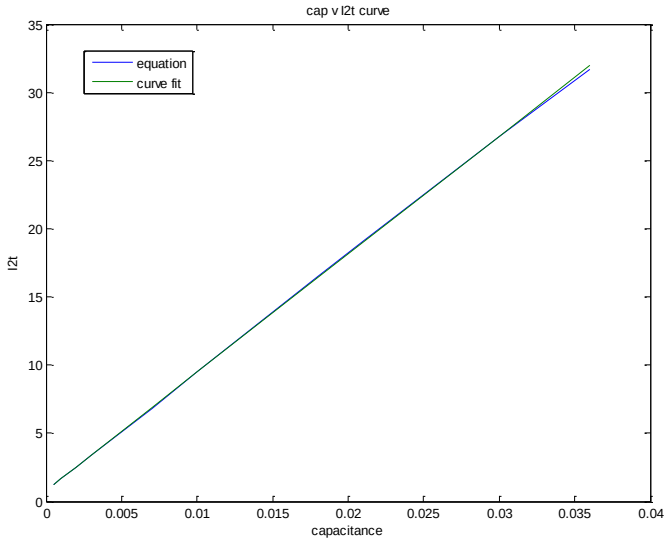

Figure 3.11: Variation of Capacitance with I^2t

Using the derived data a curve, the following equation was determined by the least squares approximation.

$$C = (E - 1.229)/866 + 5 * 10^{-4} \tag{3.7}$$

Again, E is equal to the system's I^2t value. As can be seen from Figure 13, the curve fit is almost perfect with a sum-of-squares error equal to 0.147. This equation was derived for the following parameter set:

L	1e-4 H
a (L2)	2.7e-6 H
R (load)	10 ohms
Vout	13 V
If,max	9 amps

Table 3.3: Parameter Set

While the parameters of equation (3.7) are expected to change when values in Table 3.3 are changed, the relationship between capacitance and the I^2t value is expected to remain linear. Figure 13 and equation (3.7) are very interesting results that warrant future studies. Future work should investigate how the numbers in equation (3.7) vary when values in Table 3.3 change. If a general linear relationship between capacitance and I^2t values can be written in terms of the systems parameters, then the process of determining the sufficient capacitance will be greatly simplified.

Chapter 4: Determination of a -Parameter

4.1 Equivalent Circuits

To determine the analytic solution for the fault current (2.16), it was assumed in Chapter 3 that a parallel fault could be modeled as a variable resistor in parallel with the load and having the form given in equation (2.3) and repeated here for convenience:

$$R_f = \frac{a}{t\prime - t_f} \equiv \frac{a}{t} \tag{2.3}$$

This chapter serves to justify this assumption and shows that a is equal to the inductance of the line that caused the fault. To start, consider the short circuit model given in Figure 4.1.

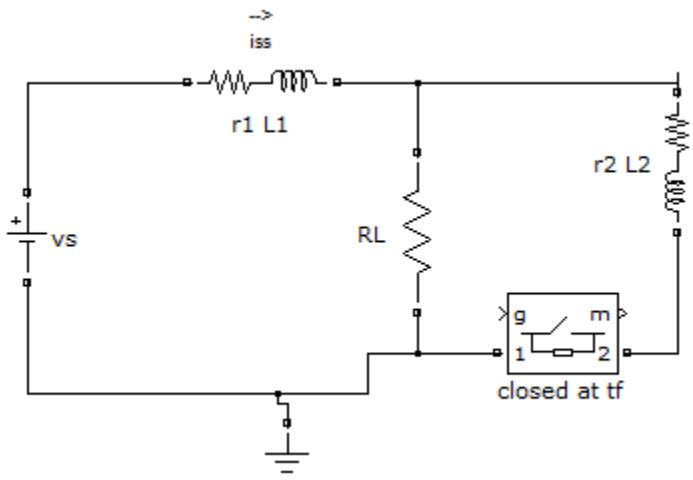

Figure 4.1: General Circuit

In this circuit, R_L is a resistive load while R_1, L_1, R_2, L_2 are the line parameters of the transmission line and fault line. The voltage source, V_s, is an idealization of the output capacitor voltage before and immediately after the fault. The switch will close at $t = t_f$. The following three assumptions can be made about this circuit:

$$R_L \gg R_1,\ R_2 \tag{4.1}$$

$$\frac{R_1}{R_2} = \frac{L_1}{L_2} = k \tag{4.2}$$

$$i_{ss}(t_f{}^-) = \frac{V_s}{R_L} \tag{4.3}$$

Inequality (4.1) states that the resistance of the load is a few orders of magnitude greater than the resistances of the transmission lines. Equation (4.2) expresses the idea that line resistance and line inductance scale linearly with distance. The justification for this is that line impedance is often expressed as impedance per unit meter. Equation (4.3) is true since V_s is a DC voltage and the inductor acts like a short circuit to DC. Inequality (4.1) implies that R_1 need not be included in the denominator of (4.3).

This circuit has two equivalent circuits which correspond to times before and after the switch is closed. The cases $t < t_f$ and $t > t_f$ are shown if figures 5.2 and 5.3 respectively.

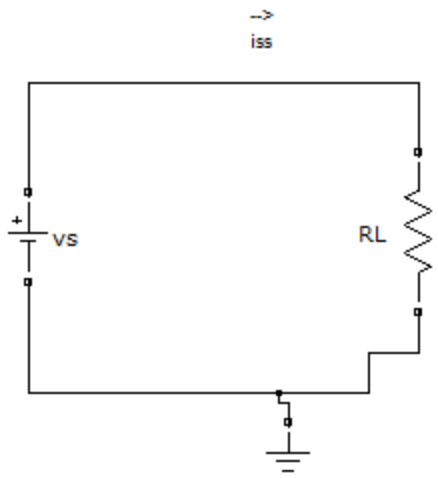

Figure 4.2: Equivalent Circuit

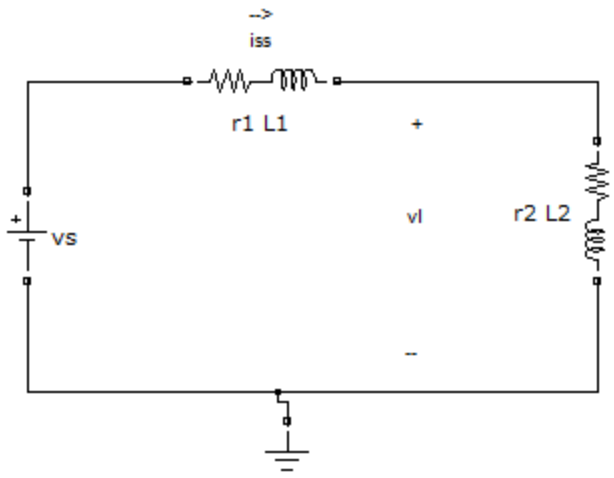

Figure 4.3: Equivalent Circuit

4.2 Circuit Differential Equations and Solutions

The absence of R_L in Figure 15 is a consequence of inequality (4.1). Since R_L is much greater than R_2, almost all of the current will flow through the R_2 branch. The differential equation for the circuit in Figure 15 is given in equation (4.4).

$$V_s = (R_1 + R_2) * i + (L_1 + L_2) * \frac{di}{dt} \tag{4.4}$$

Writing this in a separable form gives:

$$dt = \frac{(L_1+L_2)}{V_s-(R_1+R_2)*i} di \tag{4.5}$$

Integrating yields:

$$t = \frac{-(L_1+L_2)}{(R_1+R_2)} \ln|V_s - (R_1 + R_2) * i| + A \tag{4.6}$$

where A is a constant. Solving for $i(t)$ gives the following form:

$$i(t) = \frac{V_s}{R_1+R_2} + A * \exp(-b * t) \tag{4.7}$$
$$b = \frac{R_1 + R_2}{L_1 + L_2}$$

This equation assumes for simplicity that t_f=0. If not, then all of the t's would change according to: $t \rightarrow t - t_f$. Equation (4.3) can now be applied to determine A.

$$i_{ss}(0^-) = \frac{V_s}{R_L} = \frac{V_s}{R_1+R_2} + A \tag{4.8}$$

$$A = V_s * \left(\frac{R_1+R_2-R_L}{(R_1+R_2)*R_L}\right) \approx -\frac{V_s}{(R_1+R_2)} \tag{4.9}$$

Together with (4.7) gives the solution:

$$i(t) = \frac{V_s}{R_1+R_2}(1 - \exp\left(-\frac{R_1+R_2}{L_1+L_2} * t\right)) \tag{4.10}$$

Note that $i(t) = 0$ and $t \to \infty$ implies $i \to \frac{V_s}{R_1+R_2}$ which are the expected boundary conditions for the current through R_2.

Next, the KVL equation for voltage across the resistive load, v_L, can be written.

$$v_s = R_1 * i + L_1 \frac{di}{dt} + v_L \tag{4.11}$$

Rewriting gives:

$$v_L = -R_1 * i - L_1 \frac{di}{dt} + v_s \tag{4.12}$$

Substituting equation (4.10) and its derivative for i yields:

$$v_L = -R_1 * \frac{V_s}{R_1+R_2}(1 - \exp(-b * t)) - L_1 \frac{V_s}{L_1+L_2} * \exp(-b * t) + v_s \tag{4.13}$$

Rearranging:

$$v_L = \left(v_s - R_1 * \frac{v_s}{R_1+R_2}\right) + \left(R_1 * \frac{V_s}{R_1+R_2} - L_1 \frac{V_s}{L_1+L_2}\right) * \exp(-b * t) \tag{4.14}$$

$$v_L = v_s * \left(\frac{R_2}{R_1+R_2}\right) + v_s * \left(\frac{R_1*L_2-R_2*L_1}{(R_1+R_2)*(L_1+L_2)}\right) * \exp(-b * t) \tag{4.15}$$

Note from equation (4.2) $R_1L_2 - R_2L_1 = kR_2L_2 - R_2kL_2 = 0$ which implies that the second term in (4.15) is zero. Hence:

$$v_L = v_s * \left(\frac{R_2}{R_1+R_2}\right) \tag{4.16}$$

So when (4.2) is true the circuit acts as a voltage divider. Dividing (4.10) into (4.16) gives the equivalent variable resistance of the faulted line:

$$R_f = \frac{\left(\frac{R_2}{R_1+R_2}\right)}{\frac{1}{R_1+R_2}\left(1-\exp\left(-\frac{R_1+R_2}{L_1+L_2}*t\right)\right)} \tag{4.16}$$

Simplifying:

$$R_f = \frac{R_2}{\left(1-\exp\left(-\frac{R_1+R_2}{L_1+L_2}*t\right)\right)} \tag{4.18}$$

When $t < \frac{L_1}{R_1}$ the expression $\exp\left(-\frac{R_1+R_2}{L_1+L_2} * t\right)$ can be Taylor expanded, proving the claim.

$$R_f = \frac{R_2}{1-\left(1-\frac{R_1+R_2}{L_1+L_2}*t\right)} = \frac{R_2}{\frac{R_1+R_2}{L_1+L_2}*t} = \frac{R_2}{\frac{aR_2+R_2}{aL_2+L_2}*t} = \frac{L_2}{t} \tag{4.19}$$

This confirms the claim that the equivalent resistance has the form given in (2.3) and that the a parameter is the inductance of the faulted line. This result was confirmed with the Simulink® model found in Appendix B.

As seen in the two graphs in Figure 4.4, the match between the simulated solution of the equivalent parallel resistance and the resistance computed from equation (2.3) is nearly perfect.

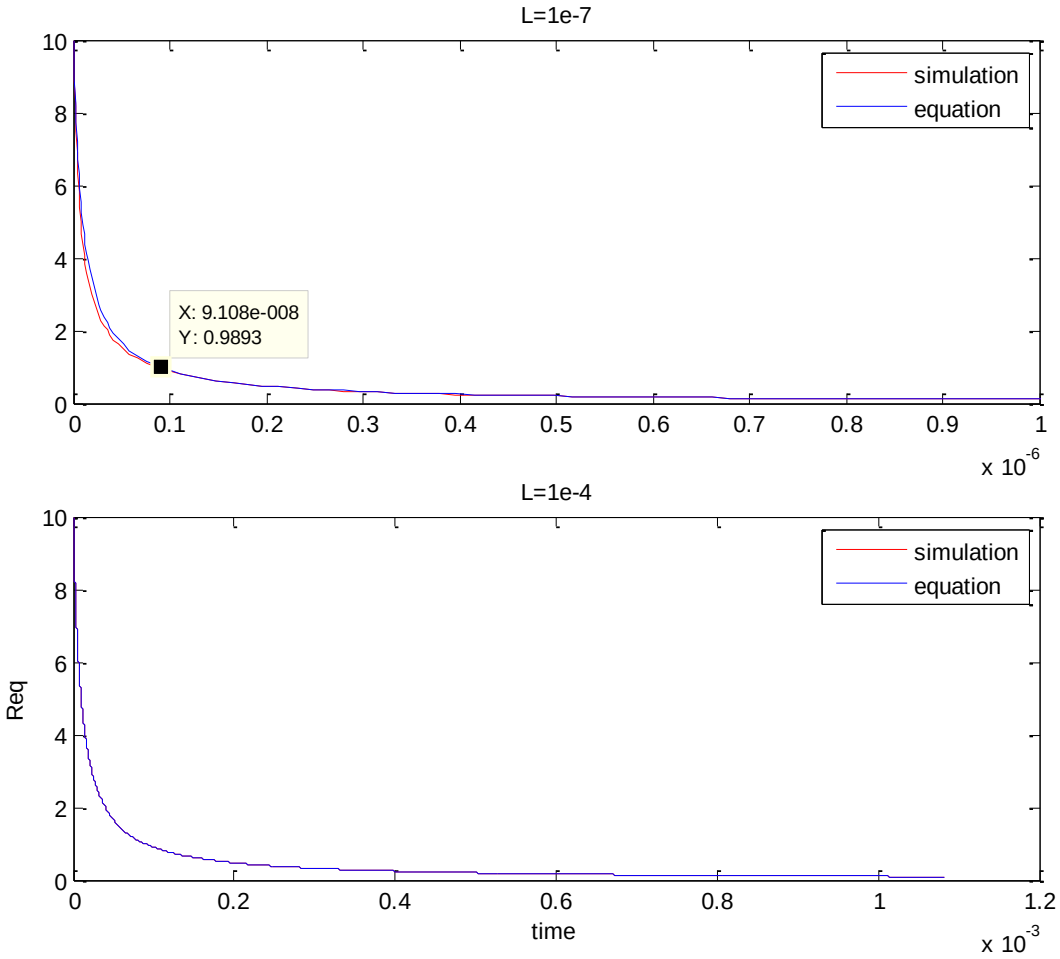

Figure 4.4: Equivalent Resistance

Even though the Taylor expansion is only valid for $t < \frac{L_1}{R_1}$, the result is approximately valid for all time since the equivalent resistance should reduce to R_2, which is close to zero, consistent with (4.19) for all practical purposes.

Chapter 5: Experimental Results

5.1 Experimental Setup

In order to empirically confirm these results, the following experiment was designed and tested. A Buck Converter with a PI control and ten ohm load resistance was constructed. A current limiter was designed to limit the amount of current flowing through the inductor in the event of a short circuit. The general scheme is shown in Figure 5.1. A picture of the physical model is shown in Appendix E.

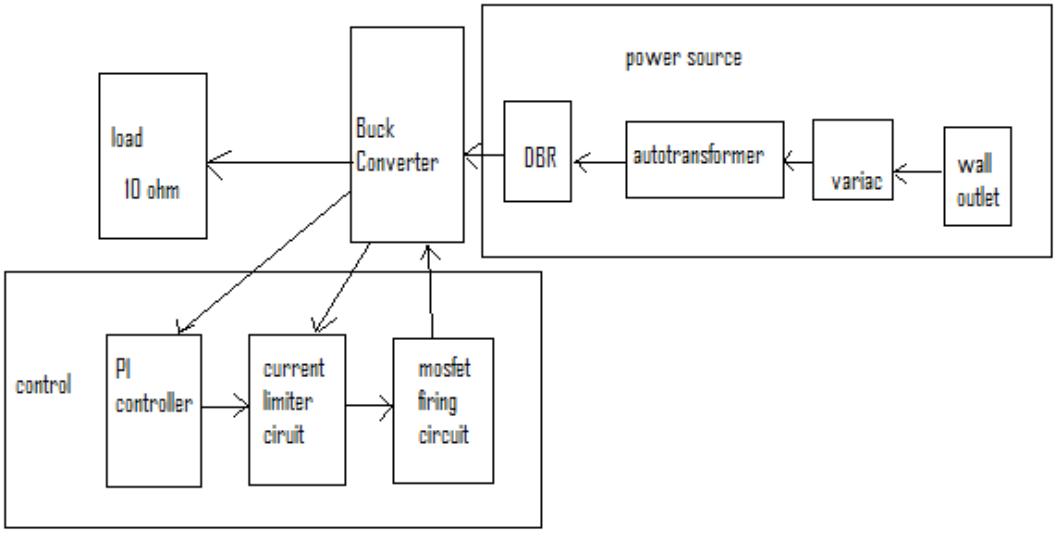

Figure 5.1: Experimental Setup

The PI controller regulates the output capacitor voltage to a preset value. It feeds into the current limiter which acts as a buffer during steady state operation. The current limiter in turn feeds into a MOSFET firing circuit which controls the duty cycle of the Buck Converter. Since the converter is a Buck Converter, two drivers and an opto-

coupler were required in the firing circuit to ensure grounding isolation. This had the effect of inverting the duty cycle: when the PWM in the firing circuit had a high input, the MOSFET opened; when it registered a low input, it closed.

5.2 Current Limiting Circuit Design

The current limiter limits the inductor current by forcing the PWM input to high when the inductor current reached a predetermined value, thereby opening the MOSFET. It accomplished this goal as follows: A 0.1 ohm shunt resistor was placed in series with the inductor in the Buck Converter. The voltage across the resistor was fed into two voltage dividers with two wires. The difference of the outputs of the two voltage dividers is still the voltage differential across the 0.1 ohm resistor, but each voltage is scaled down with respect to ground. These two scaled-down voltages are then fed to two voltage-following op-amps where the relative signal is buffered. These two signals are then fed into a differential amplifier. The differential amplifier computes the voltage difference and inputs the difference to a comparator which compares the value to a reference voltage set by a potentiometer. If the input voltage is higher than the reference voltage the comparator will output high. If the input voltage is lower than the reference voltage it will output low. The reference value can be calibrated to the maximum allowable current that passes through the inductor. The output of the comparator is then fed into the lower rail of a voltage following op-amp. The input to this op-amp is the PI control and the output feeds into the PWM. When the comparator outputs a high voltage the low rail of the buffer op-amp goes high, forcing the output to high. The PWM then receives a high voltage and opens the MOSFET. A low value from the comparator sets the low rail of the

buffer op-amp to zero and the PI controller is able to control the input to the PWM. The circuit diagram is shown in Figure 5.2.

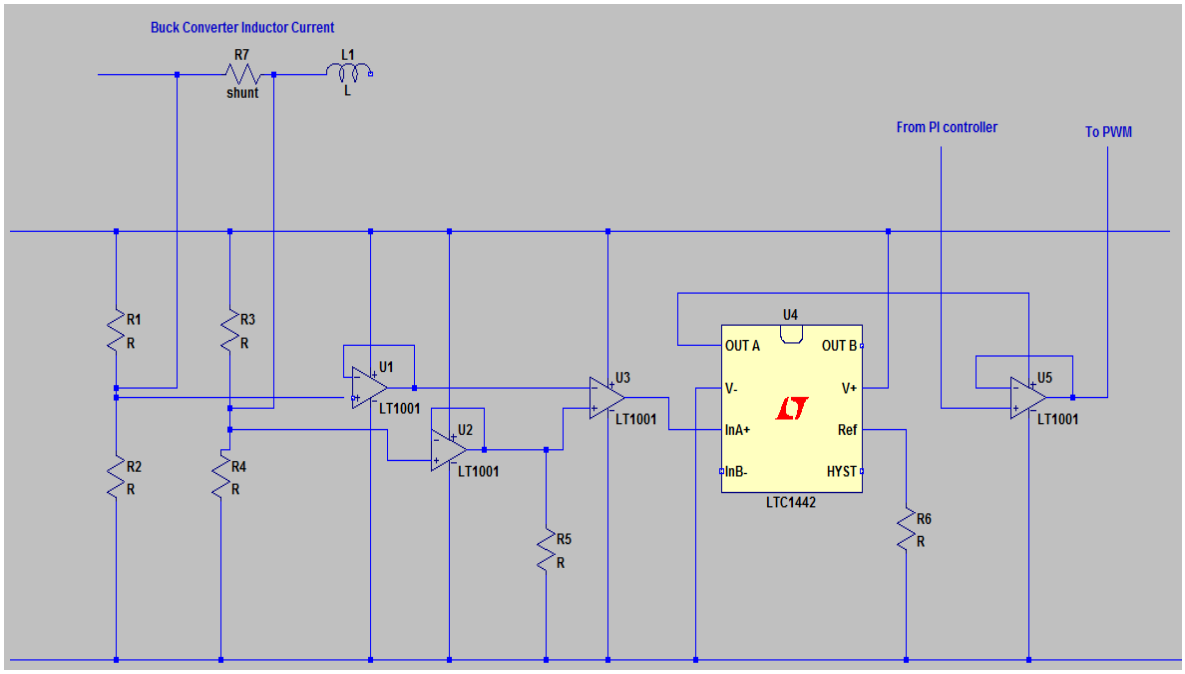

Figure 5.2: Current Limiter

Figure 5.3 shows the inductor current increasing to a maximum value of 6 amps after a short circuit occurs. In this picture, the blue graph is the inductor current and the green graph is low rail of the buffer op-amp in the current limiting circuit. Note that when the low rail goes high the inductor current saturates at its maximum value.

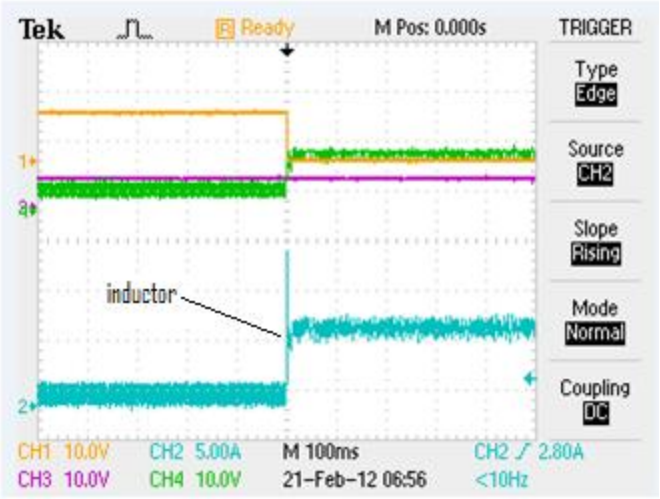

Figure 5.3: Inductor Current

5.3 Experimental Fault Simulation

Creating the fault posed an initial problem. The first attempt involved using a mechanical toggle switch to short out the load. However, this had the problem of mechanical ringing as seen in Figure 5.4.

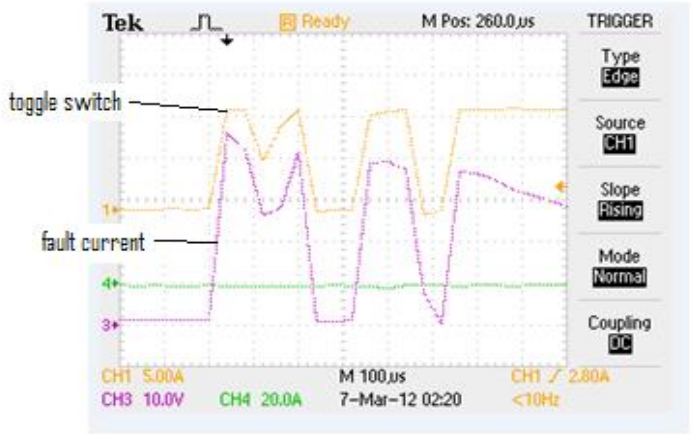

Figure 5.4: Toggle Switch Ringing

The orange graph is the toggle switch which has a ringing effect due to imperfections in the switch. The red graph is the fault current which is observed to follow the ringing in the toggle switch. To try to reduce the problem of ringing, a MOSFET was used to create a short across the load. This had the effect of reducing the ringing, however, MOSFET's have a lot of capacitance between the source and drain. This property significantly reduced the fault current adding an effect not accounted for in the theory. The third method was to use a simple hand switch. Due to the hand switch's simplicity, the ringing effect that the toggle switch had was minimized and negligible capacitance was measured. The hand switch along with its connecting wires did have a inductance equal to 2.70 micro-Henry which, from Chapter 5, is the value of L_2. A graph of the load voltage during a short is shown in Figure 5.5.

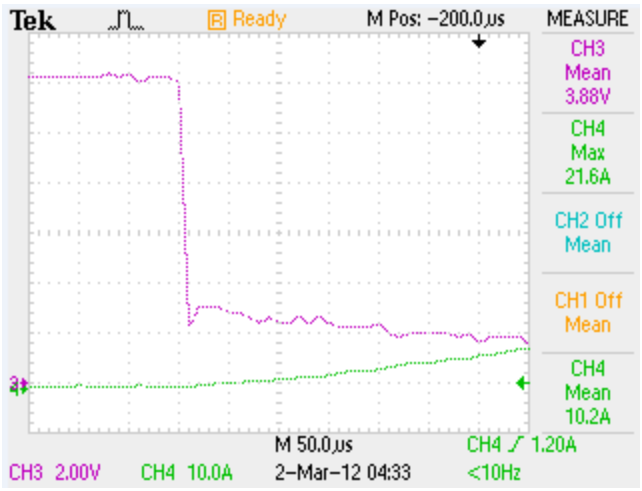

Figure 5.5: Load Voltage During Fault

From this graph it is evident that the voltage decreases to about two volts in ten microseconds. It then takes a very long time to decrease to one volt as seen in Figure 5.6. The red graph is the load voltage against time.

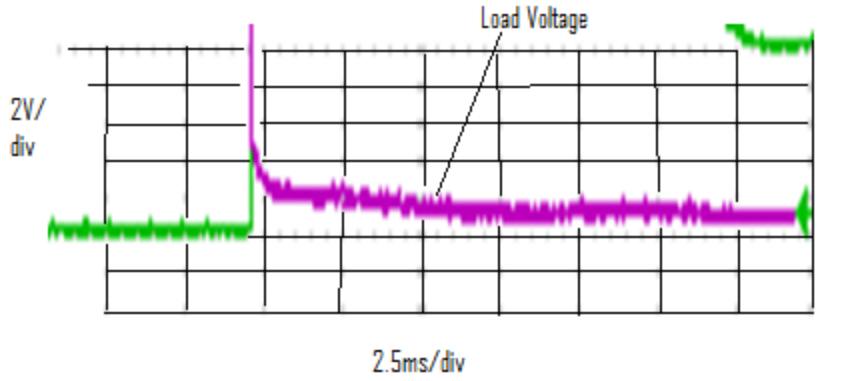

Figure 5.6: Load Voltage

The time division is 2.5ms/div while the voltage is 2V/div. It therefore takes a long time to reach one volt. This can be compared with Figure 5.7 which shows a plot of the expected short circuit voltage.

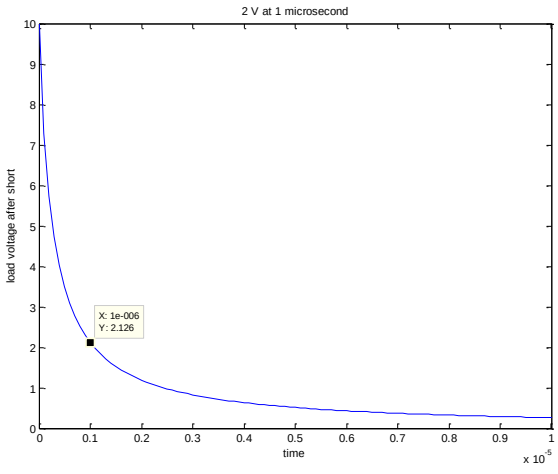

Figure 5.7: Fault Current Simulation

The voltage expected from equation (5) gives two volts after one microsecond which is ten times faster than what the experiment seems to show. The period of time it takes to decrease from two volts to under one volt is much longer than what was measured in simulation. One explanation for this is since the time division in Figure 5.5 is in units of fifty microseconds, it is not really clear what the actual time value is. A closer measurement would need to be observed. Secondly, there are most likely many small parasitic impedances in the experiment that are not accounted for in the model. For instance, when a 0.2 ohm resistor is connected in series between the output capacitor and load, the amplitude of the fault current is reduced to less than half of its original value. Figure 5.8 shows the fault current with the 0.2 ohm resistor inserted. This can be compared to Figure 5.9 which shows the fault current without the 0.2 ohm resistor.

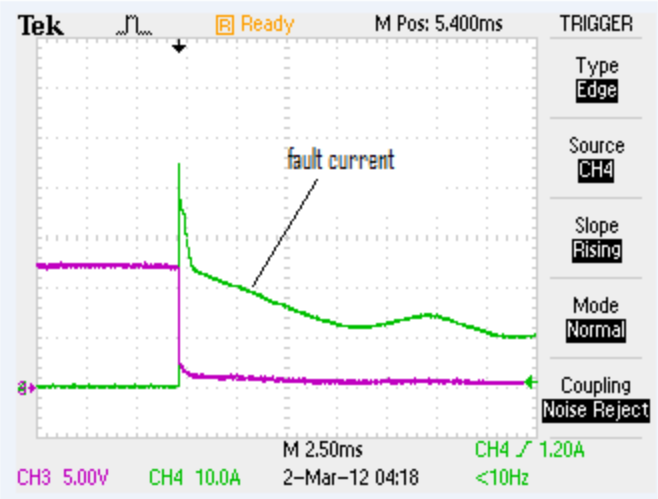

Figure 5.8: Fault Current with 0.2ohm Resistor

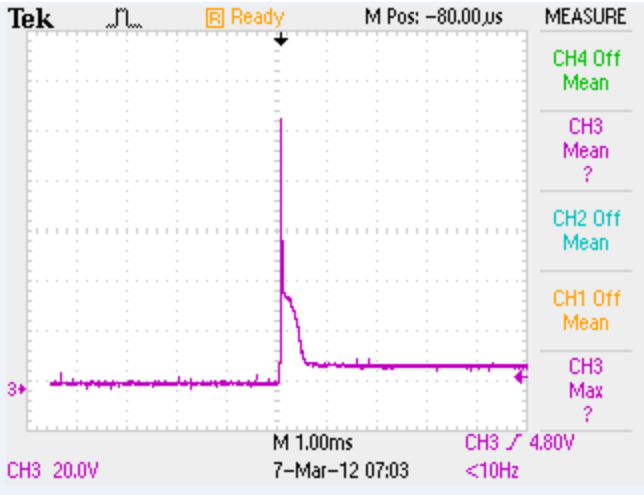

Figure 5.9: Fault Current without 0.2 ohm Resistor

In Figure 5.8, the amplitude of the fault current is about 45 V and takes over 17 milliseconds to reach steady state. In Figure 5.9, the amplitude of the fault current is about 105 V and takes less than a millisecond to reach steady state. This shows that the experimental model is extremely sensitive to parameter variation. One reason for this may be due to the low voltages and low load resistances used. At higher voltages and load resistances it is reasonable to expect that these parasitic impedances will become more negligible. However, for safety reasons the experiment is conducted at low voltage.

5.4 The Experiment

The experiment first consists of calculating the I^2t value that the Buck Converter can deliver to a fuse. If this value is greater than the I^2t rating of the fuse, then the fuse should blow very quickly. If the calculated value is lower than the rated value but the maximum allowable current is greater than the fuse current rating, then the fuse should blow, but much more slowly. If the computed I^2t is less than the rated value and the fuse

current rating is less than the maximum allowable current, then the fuse is expected not to blow. The following Table gives the initial parameters of the experiment.

Vin	20 V
Vout	13 V
Rload	10 ohms
C (output)	3 mF
L (main)	100 microH
L_2	2.7 microH
Line resistance	0.11 ohms
Switching frequency	120 khz
Current limit	9 amps

Table 5.1: Experimental Parameter Values

The first test that was conducted was to determine if the fault current matched the current predicted by the theory. Figure 5.9 shows the actual fault current measured with an oscilloscope while Figure 5.10 shows the theoretical fault current.

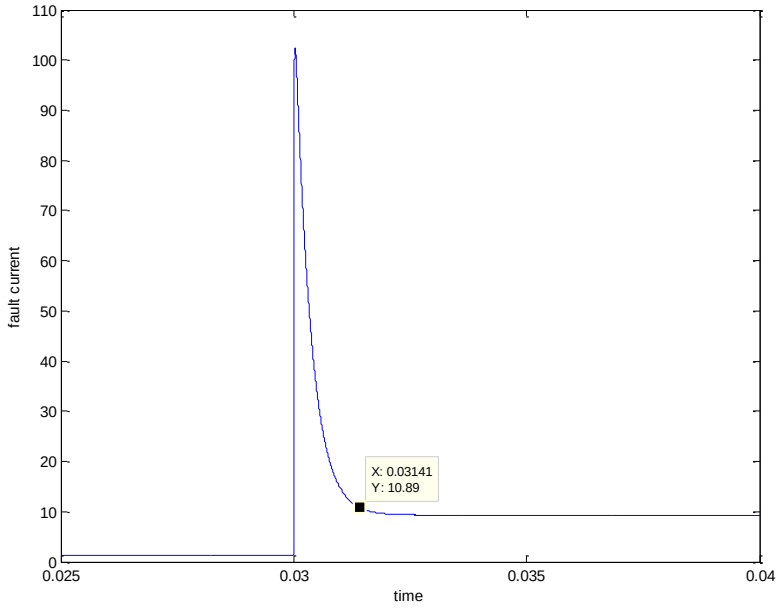

Figure 5.10: Simulation Fault Current

As can be seen from the two graphs, Figure 5.9 and 5.10, the peaks are approximately 105 V. The experimental graph takes less than one millisecond to reach steady state while the theoretical graph takes just over one millisecond. The experimental graph also has a sudden concave down portion while the theoretical graph is always concave up. The difference again may be due to unaccounted for parasitic impedances that have effects due to relatively low parameter values mentioned above. Another explanation is that the PI controller and current limiter were not optimally designed. The simulation assumes an ideal controller. However, for all practical purposes, the graphs seem close.

"Shurter" fast-acting fuses were used in this experiment. These fuses have low I^2t values making them ideal for experiments with low voltages. The published Table of I^2t

values for given rated current values is shown in Appendix C. Table 5.2 lists the results of the experiment when the output capacitance is 3.3 milli-Farads.

Rated current	Rated I^2t	Computed I^2t	Result
.5	.044	3.374232258	Blown (before fault)
1.6	.94	3.374232258	Blown (immediately after fault)
2	1.3	3.374232258	Blown (immediately after fault)
2.5	1.9	3.374232258	Blown (immediately after fault)
3.15	5.4	3.374232258	Blown (more than 1 second after fault)
5	11.2	3.374232258	Not blown

Table 5.2: Experimental Results

The average steady state load current prior to the fault is 1.3 amps. When the 0.5 amp fuse was used the fuse melted immediately, before the fault was initiated. In the case of the 1.6 to 2.5 amp fuses the melting occurred immediately after the fault was initiated. For the 3.15 amp fuse, the fuse melted but it took a few seconds. This is because the I^2t value of the fuse was higher than what the converter could supply. However, since the maximum inductor current was set to nine amps and the current rating was only five amps, the fuse continued to melt after the short circuit current returned to the maximum allowed current. This phenomenon is shown in Figure 5.11.

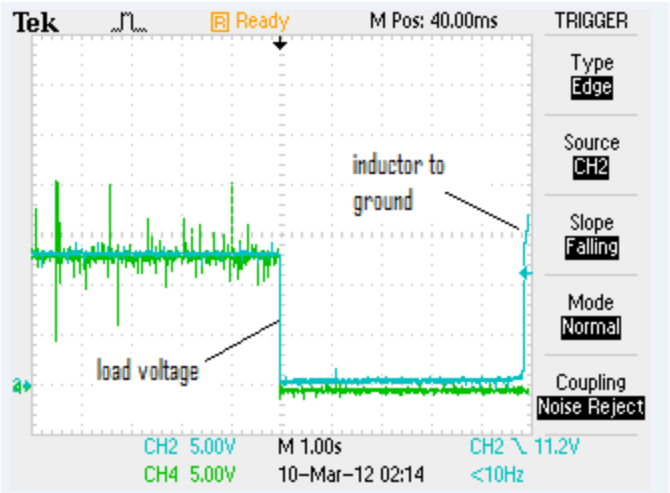

Figure 5.11: Fuse Opening

In Figure 5.11, the green graph is the load voltage and the blue graph is the inductor to ground voltage on the opposite side of the fuse. Toward the very right of the graph, after about five seconds, the fuse melts and the inductor to ground voltage rapidly increases.

The three milli-Farad capacitor was not sufficient to clear the five amp fuse. This fuse is expected to eventually melt since the average post fault steady state fuse current is nine amps. To blow the five amp fuse, the output capacitance was increased to 18,000 micro-Farads. This has an associated I^2t value equal to 16.4 which is greater than the I^2t value of the fuse. While the fuse did melt with this capacitance, it is debatable as to whether it melted fast enough. Figure 5.12 shows the voltages across the load and the voltage across the supply side of the fuse.

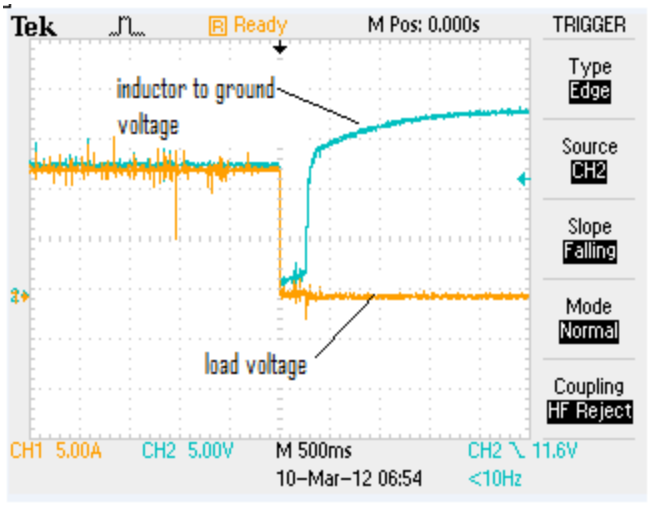

Figure 5.12: Fuse Opening

Here the orange graph is the load voltage and the blue graph is the supply side voltage. As can be seen, it takes about 250 milliseconds for the supply side voltage to recover. During this period, one can observe a brief linear increase in voltage that most likely corresponds to the links in the fuse melting. Once a sufficient number of links melt, the fuse becomes an open circuit and the voltage dramatically increases. A 21,000 micro-Farad capacitor was then used, and this melting period was observed to dramatically decrease.

Chapter 6: Alternative Formulation

6.1 Introduction

In this chapter an alternative method for computing capacitance will be presented. In the previous model, a variable resistor was used to short out the load. In this model, the short will be modeled as a line with inductance L and resistance r in parallel with the resistive load, R. While the method derived in the previous chapter has been found to be accurate within a certain parameter domain, the method presented here will be accurate for a much greater range of values. It is also a simplified method since a closed form solution for capacitance will be derived.

6.2 Circuit Model

To begin, consider the circuit shown in Figure 6.1.

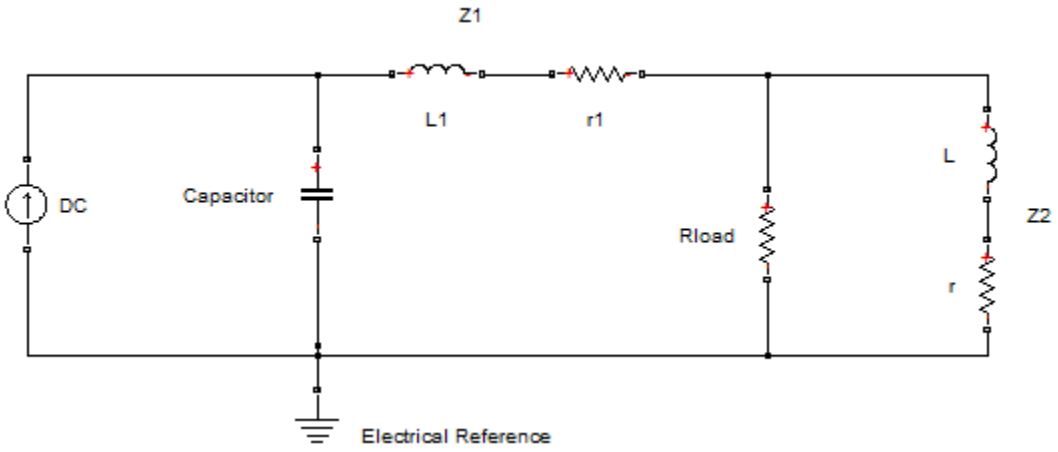

Figure 6.1: Circuit Model

This circuit models Figure 1.1 at the moment a short circuit occurs across the resistive load. In this circuit, Z_1 is the impedance of the distribution line and Z_2 is the impedance of the short circuit. R is the resistance of the load. As before, the inductor current is modeled to be approximately constant since the difference between the steady state operation and the maximum allowable current is small compared to the current spike from the capacitor. Assume the magnitude of Z_1 is small compared to R. Then the equivalent resistance seen by the fault current can be approximated as follows:

$$Z_{eq} = Z_1 + R \,||Z_2 = Z_1 + \frac{R * Z_2}{R + Z_2} = \frac{R * (Z_1 + Z_2) + Z_1 * Z_2}{R + Z_2} \approx \frac{R * (Z_1 + Z_2)}{R + (Z_2 + Z_1)}$$
$$= R \,||(Z_1 + Z_2) = R \,||Z' \qquad (6.1)$$

The approximation follows from the assumption: $Z_1, Z_2 \ll R$. Figure 6.2 gives the equivalent of 7.1. Here r and L have been changed according to equation (6.1).

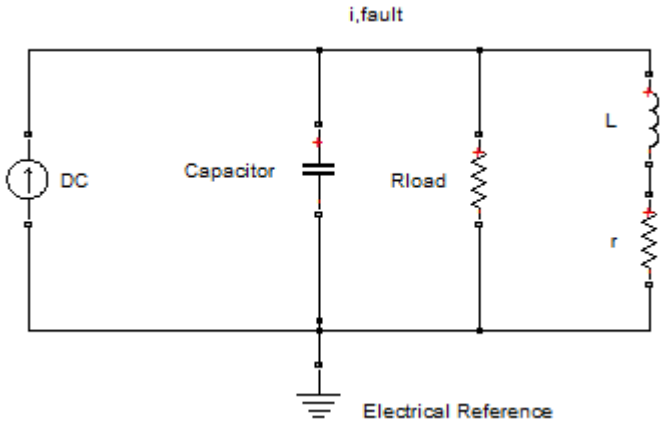

Figure 6.2: Equivalent Circuit

6.3 Derivation of I^2t Equation

The fault current will be derived using this model and has the general form given in equation (1.1). The voltage across the inductor can be expressed as:

$$v_L = -L\frac{di_L}{dt} \tag{6.2}$$

The negative sign in equation (6.2) was confirmed with simulation. Using (6.2):

$$v_L = v_c - i_L * r = -L\frac{di_L}{dt} \tag{6.3}$$

Rearranging:

$$\frac{di_L}{dt} - i_L\frac{r}{L} = -\frac{v_c}{L} \tag{6.4}$$

Using equation (2.10) gives the solution to (6.4):

$$i_L = exp\left(\frac{r}{L}t\right)\left(\int -\frac{v_c}{L}exp\left(-\frac{r}{L}t\right)dt + K\right) \tag{6.5}$$

Equation (1.1) and Figure 6.2 imply:

$$i_f = i_c + I_m = i_R + i_L \tag{6.6}$$

Here I_m is the maximum allowable current through the inductor in Figure 1.1 which corresponds to the current source in Figure 6.2. It will be shown that the calculated capacitance is insensitive to this value.

Substituting equations (1.2), (6.5) and using Ohm's law for the resistive load gives the following equation:

$$-C\frac{dv_c}{dt} + I_m = \frac{v_c}{R} - exp\left(\frac{r}{L}t\right)\left(\int \frac{v_c}{L} exp\left(-\frac{r}{L}t\right) dt + K\right) \quad (6.7)$$

Rearranging:

$$-C\frac{dv_c}{dt} exp\left(-\frac{r}{L}t\right) + I_m\, exp\left(-\frac{r}{L}t\right) = \frac{v_c}{R} exp\left(-\frac{r}{L}t\right) - \left(\int \frac{v_c}{L} exp\left(-\frac{r}{L}t\right) dt + K\right) \quad (6.8)$$

Differentiating with respect to t:

$$-C\frac{d^2v_c}{dt^2} exp\left(-\frac{r}{L}t\right) + C\frac{r}{L}\frac{dv_c}{dt} exp\left(-\frac{r}{L}t\right) - I_m\frac{r}{L} exp\left(-\frac{r}{L}t\right) = \frac{1}{R}\frac{dv_c}{dt} exp\left(-\frac{r}{L}t\right) - \frac{r}{RL}v_c\, exp\left(-\frac{r}{L}t\right) - \frac{v_c}{L} exp\left(-\frac{r}{L}t\right) \quad (6.9)$$

Canceling the $exp\left(-\frac{r}{L}t\right)$ gives:

$$-C\frac{d^2v_c}{dt^2} + C\frac{r}{L}\frac{dv_c}{dt} - I_m\frac{r}{L} = \frac{1}{R}\frac{dv_c}{dt} - \frac{r}{RL}v_c - \frac{v_c}{L}$$

Collecting terms and simplifying yields the second order linear non-homogenous differential equation:

$$RLC\frac{d^2v_c}{dt^2} + \frac{dv_c}{dt}(L - RrC) - (r + R) = -I_mRr \quad (6.10)$$

Since $r \ll R$ this can further be simplified to:

$$RLC\frac{d^2v_c}{dt^2} + \frac{dv_c}{dt}(L - RrC) - R = -I_mRr \quad (6.11)$$

6.4 Solution and Analysis

Equation (6.11) will have a general solution of the form:

$$v_c = A * exp(s_+ t) + B * exp(s_- * t) + K \tag{6.12}$$

Here, A, B, s_+, s_- and K are constants. Substituting (6.12) into (6.11) and invoking the linear independence of exponentials and constants yields two equations:

$$RLCs^2 + (L - RrC)s - R = 0 \tag{6.13}$$

$$-KR = -I_m Rr \tag{6.14}$$

The solutions are respectively:

$$s = s_\pm = \frac{(RrC-L) \pm \sqrt{(RrC-L)^2 + 4R^2LC}}{2RLC} \tag{6.15}$$

$$K = I_m r \tag{6.16}$$

An analysis of the parameters involved in (6.15) shows $A * exp(s_+ t)$ diverges to infinity. Since v_c should tend to a small finite value A must be equal to zero. Therefore, from (6.12) and (6.16):

$$v_c = B * exp(s_- * t) + I_m r \tag{6.17}$$

When $t = 0$ the capacitor voltage should equal the steady state capacitor voltage V_0, hence:

$$V_0 = B + I_m r \approx B \tag{6.18}$$

The approximation in (6.18) follows from $V_0 \gg I_m r$ in most practical situations. The capacitor voltage is finally:

$$v_c = V_0 * exp(s\_ * t) + I_m r \tag{6.17}$$

Figure 6.3 compares equation (6.17) with the capacitor voltage generated from simulation. Note that (6.17) is not valid before the time of the fault.

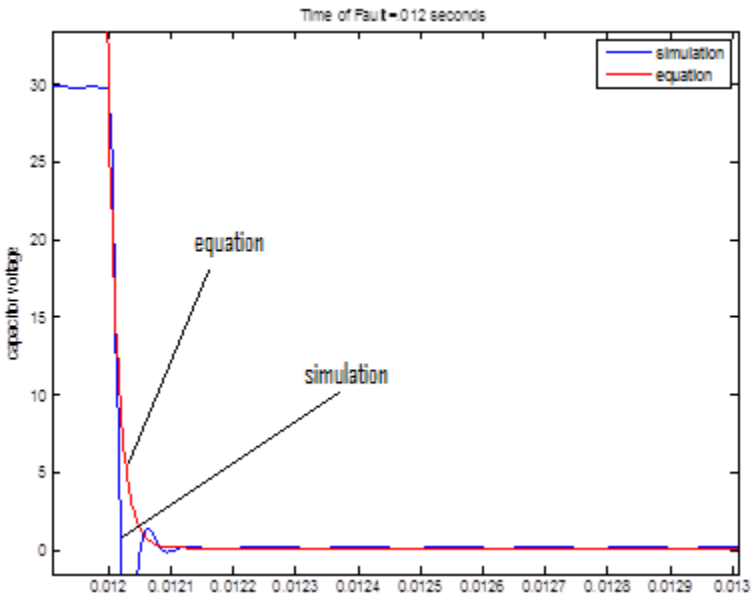

Figure 6.3: Capacitor Voltage During a Fault

It is believed that the oscillations seen in the lower left corner of Figure 6.3 are a result of modeling the line inductance as ideal elements. The following Table gives the parameter values used in some of the following simulations:

Vin	100 V
Vout	30 V
C (output filter)	1e-4 F to 5e-3 F
L (output filter)	1e-4 H
R1	20 ohms
R2	20 ohms
L (line)	1e-7 Henry
R (line)	1e-2 ohms
I_m	9 Amps
E	30 Amp^2 sec

Table 6.1: Solution and Parameter Values

The fault current can now be calculated using equation (1.1), (1.2) and (6.17).

$$i_f = I_m - CV_0 s\_ exp(s\_ t) \tag{6.18}$$

Squaring this gives:

$$i_f{}^2 = I_m{}^2 + C^2 V_0{}^2 s\_{}^2 \, exp(2s\_ t) - 2I_m CV_0 s\_ exp(s\_ t) \tag{6.19}$$

Finally, integrating both sides with respect to t yields:

$$\int_0^{t_f} i_f{}^2 dt = I_m{}^2 t + \frac{1}{2} C^2 V_0{}^2 s\_ \, exp(2s\_ t) - 2I_m CV_0 exp(s\_ t) \,|_0^{t_f} \tag{6.20}$$

For $t_f > 1$ milliseconds and for typical parameter values as found in Table 6.1, $\exp(s\_t) \approx 0$. Inserting the limits of integration into (6.20) gives:

$$\int_0^{t_f} {i_f}^2 dt = {I_m}^2 t_f - \frac{1}{2} C^2 {V_0}^2 s\_ + 2 I_m C V_0 \tag{6.21}$$

Equation (6.21) gives the I^2t value that the converter can supply to the fuse after t_f seconds assuming t_f is sufficiently large. How large t_f needs to be depends on $s\_$. For typical values as given in Table 6.1, $s\_$ is in the thousands. Note that $\frac{\partial}{\partial I_m} \int_0^{t_f} {i_f}^2 dt = 2 I_m t_f + 2 C V_0 \ll 1$ for reasonable parameter values, which implies that equation (6.21) is insensitive to values of I_m. This justifies the assumption of the constant current source shown in Figure 6.2.

6.5 Polynomial Approximations

As stated in equation (2.19), the required value of C can now be determined by finding the roots of the following function:

$$f(C) = {I_m}^2 t_f - \frac{1}{2} C^2 {V_0}^2 s\_ + 2 I_m C - E \tag{6.22}$$

Here E is the I^2t rating of the fuse. This equation is very general and can be solved with numerical techniques. However, for typical parameter values consider again equation: (6.15):

$$s = s_{\pm} = \frac{(RrC - L) \pm \sqrt{(RrC - L)^2 + 4R^2 LC}}{2RLC}$$

Analysis of the terms in this equation for typical values results in the relations:

$$\begin{aligned} RrC &\gg L \\ (RrC - L)^2 &\ll 4R^2LC \end{aligned} \tag{6.23}$$

These relations hold over a wide range of parameter values and for most practical cases. Relation (6.23) along with equation (6.15) imply:

$$s = s_{-} = \frac{r}{2L} - \frac{1}{\sqrt{LC}} \tag{6.24}$$

Substituting (6.24) into (6.22) gives:

$$f(C) = {I_m}^2 t_f - \frac{1}{2} C^2 {V_0}^2 \left(\frac{r}{2L} - \frac{1}{\sqrt{LC}}\right) + 2I_m C - E = 0 \tag{6.25}$$

After some algebra, rearrangement results in:

$$\frac{2\sqrt{L}}{V_0^2}(E - {I_m}^2 t_f) - \frac{r}{2\sqrt{L}} C^2 - \frac{4I_m\sqrt{L}}{V_0} C = \sqrt{C^3} \tag{6.26}$$

To simplify the algebra, (6.26) can be written:

$$\varepsilon_0 + \varepsilon_1 C + \varepsilon_2 C^2 = \sqrt{C^3} \tag{6.27}$$

$$\begin{aligned} \text{With,} \quad \varepsilon_0 &= \frac{2\sqrt{L}}{V_0^2}(E - {I_m}^2 t_f) \\ \varepsilon_1 &= -\frac{4I_m\sqrt{L}}{V_0} \\ \varepsilon_2 &= -\frac{r}{2\sqrt{L}} \end{aligned}$$

Squaring both sides of (6.27) and collecting terms gives:

$$\varepsilon_0^2 + 2\varepsilon_0\varepsilon_1 C + (2\varepsilon_0\varepsilon_2 + \varepsilon_1^2)C^2 + 2\varepsilon_1\varepsilon_2 C^3 + \varepsilon_2^2 C^4 = C^3 \tag{6.28}$$

This can be written more efficiently as:

$$\alpha_0 + \alpha_1 C + \alpha_2 C^2 + \alpha_3 C^3 + \alpha_4 C^4 = 0 \tag{6.31}$$

Here, the α_i's are functions of the ε_i's which in turn are functions of the system parameters. After some algebra the α_i's can be directly written in terms of the system parameters.

$$\alpha_0 = \frac{4L}{V_0^4}(E - I_m^2 t_f)^2 \tag{6.32}$$

$$\alpha_1 = \frac{-16 I_m L}{V_0^3}(E - I_m^2 t_f) \tag{6.33}$$

$$\alpha_2 = \frac{2r}{V_0^2}\left(E - I_m^2 t_f\right) + \frac{16 I_m^2 L}{V_0^2} \tag{6.34}$$

$$\alpha_3 = \frac{-4 r I_m}{V_0} - 1 \tag{6.35}$$

$$\alpha_4 = \frac{r^2}{4L} \tag{6.36}$$

Equation (6.31) is a fourth order polynomial in C with coefficients given by (6.32)-(6.36). The solution to (6.31) will be the minimum capacitance required to melt a fuse with $E = I^2 t$. A closed form solution can therefore be written for (6.31), though this would be needlessly complex. Simulations show that for parameters that may be considered practical, equations (6.32) and (6.33) are approximately zero. This means that (6.31) can be reduced to a second order polynomial equation:

$$\alpha_2 + \alpha_3 C + \alpha_4 C^2 = 0 \tag{6.37}$$

The solution is given by:

$$C = \frac{\frac{4 r I_m}{V_0} + 1 \pm \sqrt{\left(\frac{4 r I_m}{V_0} + 1\right)^2 - \frac{2 r^3}{L V_0^2}(E - I_m^2 t_f)}}{\frac{r^2}{2L}} \tag{6.38}$$

This solution is only valid when the discriminant is greater than or equal to zero:

$$(\frac{4rI_m}{V_0}+1)^2-\frac{2r^3}{LV_0^2}\left(E-I_m^2t_f\right)\geq 0 \tag{6.39}$$

Solving this inequality for E gives:

$$E<I_m^2t_f+\frac{LV_0^2}{2r^3}(\frac{4rI_m}{V_0}+1)^2\approx\frac{LV_0^2}{2r^3} \tag{6.40}$$

Inequality (6.40) states that the maximum E-value for which equation (6.38) will remain valid is equal to $\frac{LV_0^2}{2r^3}$. Figure 6.4 shows how the discriminant in equation (6.38) varies with E.

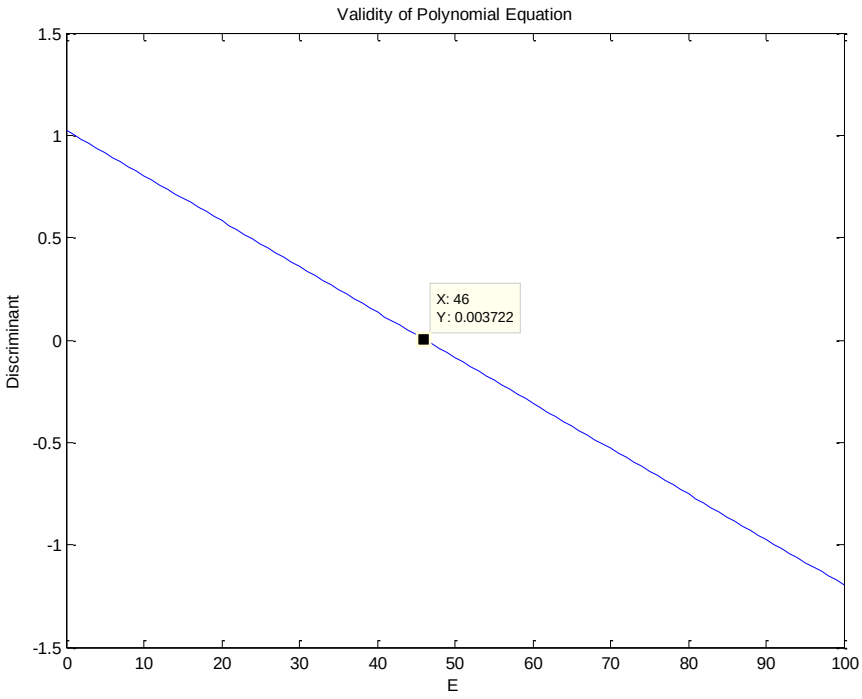

Figure 6.4: Discriminant versus E

From the graph it is seen that the discriminant is zero when E is approximately 46. This can be compared to graphs of the polynomial function (6.31).

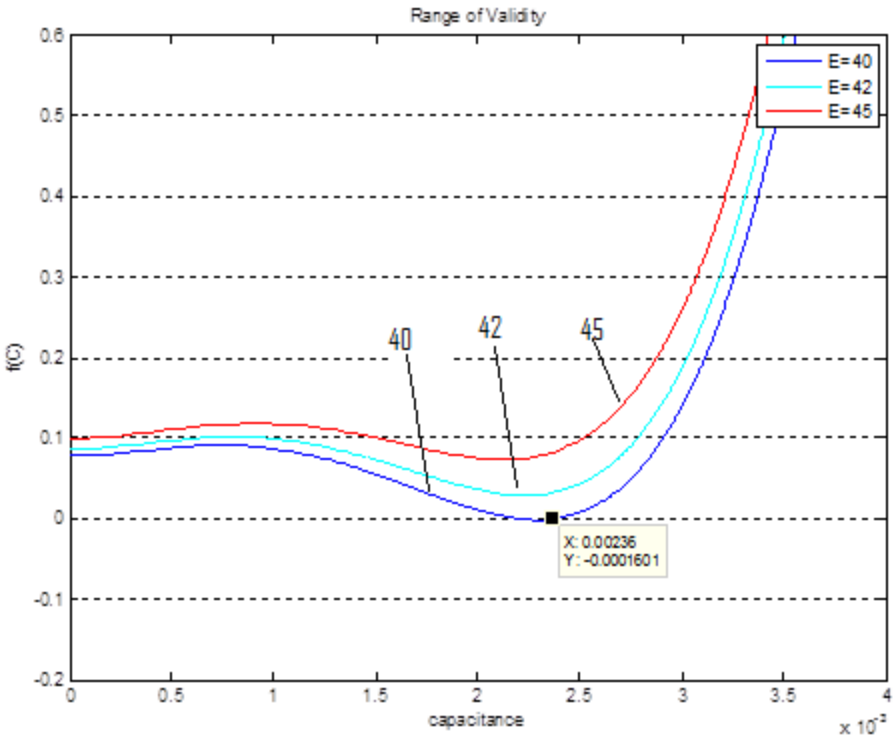

Figure 6.5: Polynomial Equations Parameterized by Capacitance

This graph shows that the maximum value for which equation (6.31) has a solution is $E = 40$ when the parameters are specified by Table 6.1. The corresponding capacitance is $C = 2.3mF$. This implies that inequality (6.40) is a necessary but not a sufficient condition.

Figure 6.6 shows a graph of equation (6.31) for the parameter set given in Table 6.1.

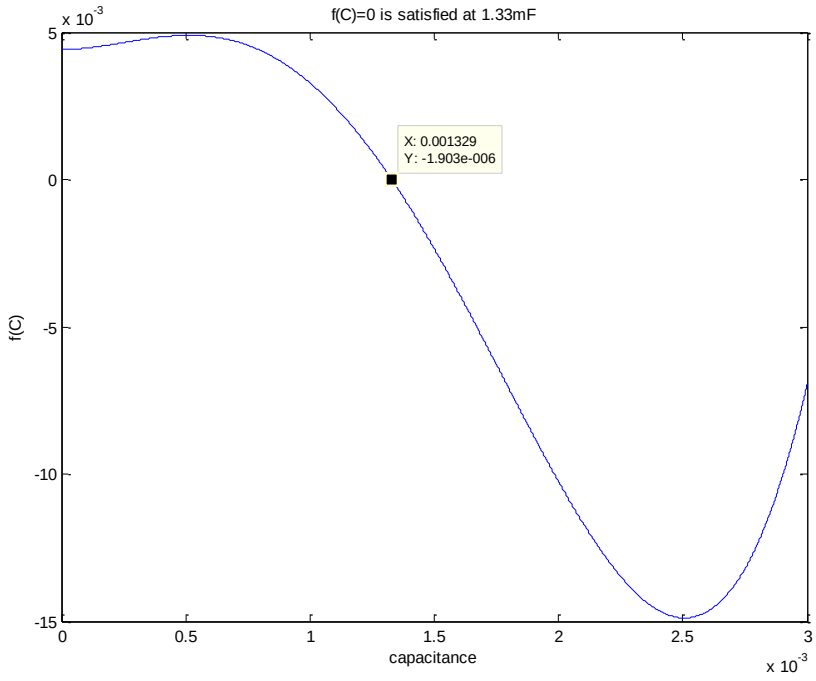

Figure 6.6: Solution of Polynomial Equation for E=30

A solution is found at $C = 1.33mF$. As implied by the graph, another solution exists. Equation (6.31) may have up to four solutions; one way to determine if the solutions are correct is to plug them into the first derivative of equation (6.22). The correct value will have a positive first derivative. Observations of many graphs like Figure 6.6 indicate that the equations will likely have at most two unique real roots.

Simulations show that $C = 1.33mF$ is an overestimate and that $.8mF$ is the required capacitive value. I^2t graphs for various capacitive values for the case $E = 30$ are shown in Figure 6.7.

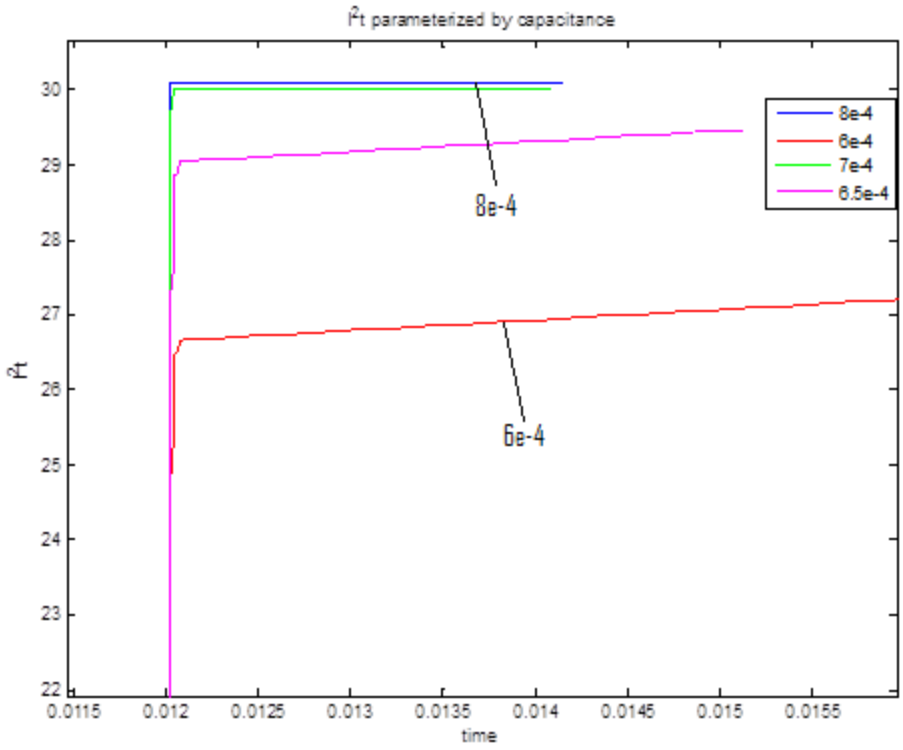

Figure 6.7: I^2t graphs for E=30

The $E = 20$ case is shown in Figure 6.8.

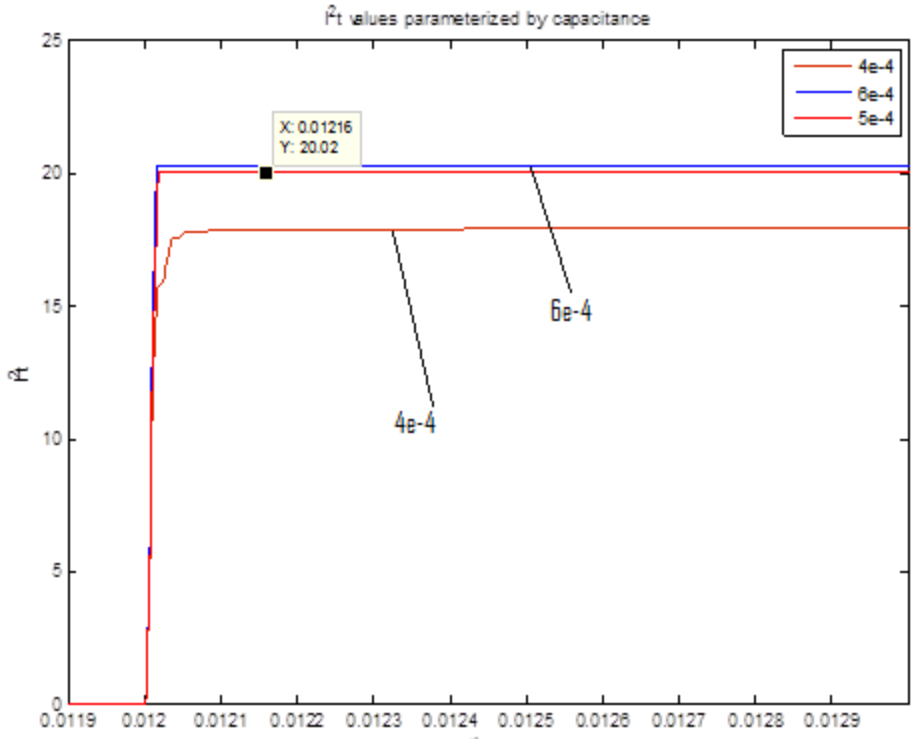

Figure 6.8: I^2t graphs for E=20

Here $C = .6mF$ was sufficient to clear the fuse. The next plot shows a comparison of the general integral equation (6.25) with the fourth order polynomial equation (6.31) and the second order approximation (6.37) for the case $E = 20$. From the graph it is seen that there is a root at .868mF and a root at 3.53mF. All three equations agree on the upper root. The derivative of the upper root is seen to be positive and is therefore the correct value.

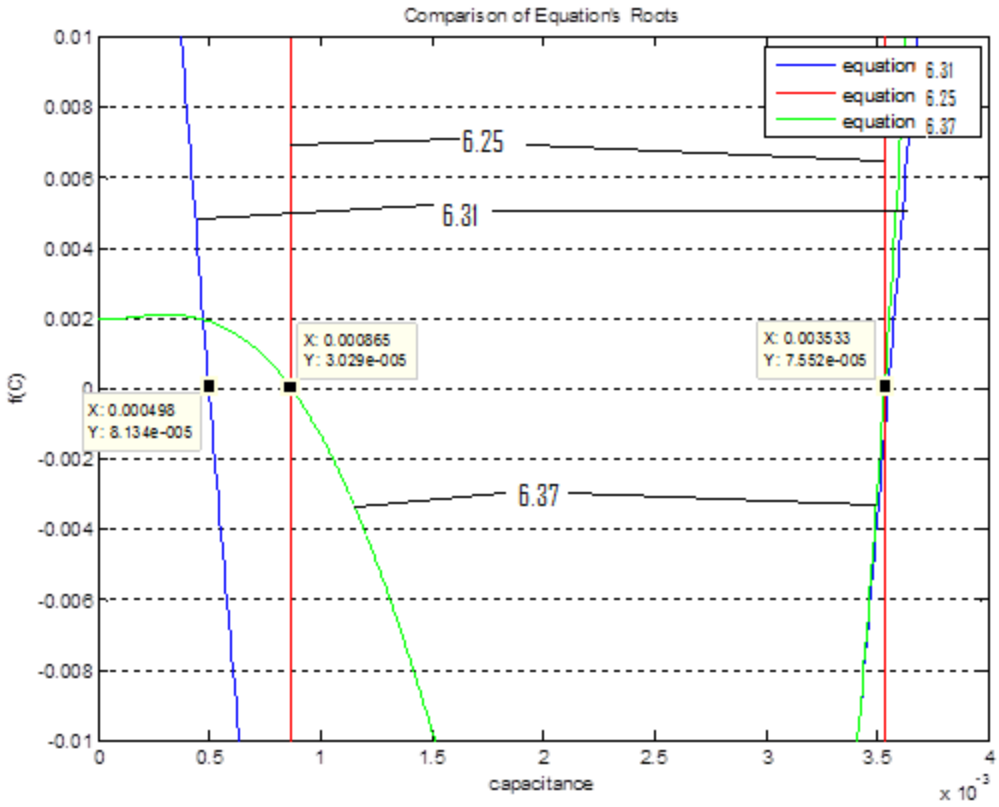

Figure 6.9: Comparison of Equation Roots

It is believed that any differences between theory and simulation are a result of the simulation having many different contingencies. The final graph shows the voltage recovery profile for R2 for three different capacitive values.

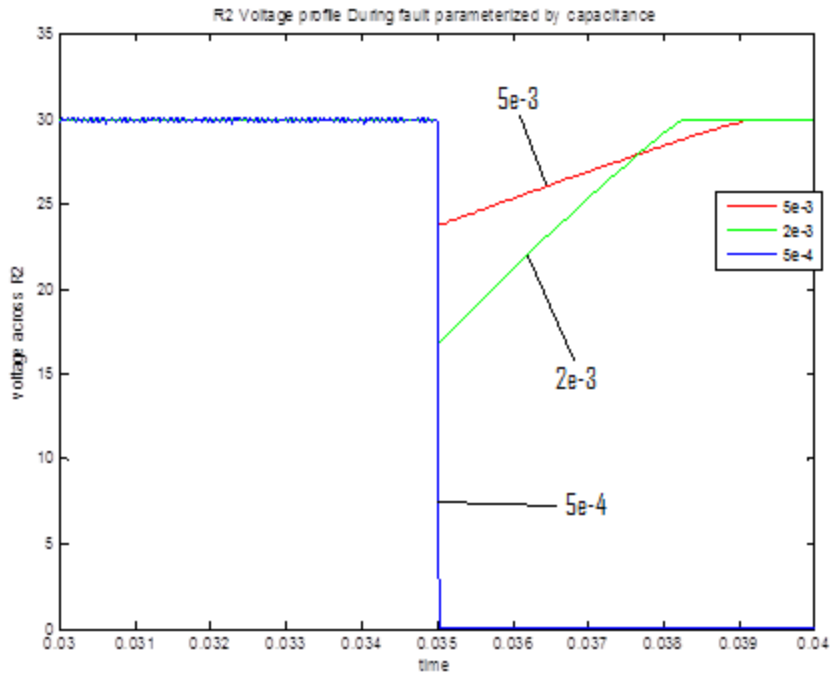

Figure 6.10: R2 Voltage Profile During Fault, Parameterized by C

In this plot, $E = 30$. As can be seen, $C = .5mF$ was insufficient to clear the fault. $C = 2mF$ cleared the fault completely after 3 milliseconds and 5 mFenabled the voltage to return to steady state after 4 milliseconds. However, the larger capacitor only allowed the voltage to drop 5 volts while the smaller capacitor allowed the voltage to drop almost 15 volts.

Chapter 7: Conclusion

Two formulations were derived to compute the idealized fault current for parallel faults with a power converter. In both cases, the time integral of the fault current squared can be calculated and compared to fuse values published by fuse distributors. This can be used to determine the amount of capacitance required to melt the fuse in the case of a fault. In the first case, a correction to the lower limit of the I^2t integral is required to correct simplifying assumptions about the inductor current. An equation for this lower limit has been estimated using the curve fitting solver in Microsoft® Excel. A closed form solution in terms of capacitance and inductance has been derived. This equation, however, has been found to be limited in scope, depending on system parameters that were not taken into account when deriving it. In particular, the correction to t_0 was found to be dependent on the inductance of the shorting line, L_2. An additional analysis was performed for L_2<10^{-6} H with the result that t_0 could be approximated to be roughly equal to 1.25e-8 for a certain range of output capacitance. The extreme sensitivity the fault current has to t_0 is a result of multiplying arbitrarily small numbers to arbitrarily large numbers. The practical employment regarding some of the equations derived in the first method is therefore limited. Further exploration concerning the linear relationship between the I^2t values and output capacitance as expressed in equation (3.7) may be a way forward.

As an answer to some problems with this method, a second method was developed. In this method, a closed form equation relating the amount of capacitance to the I^2t value of the fuse was derived. Certain assumptions allowed this general equation to be reduced to a fourth order polynomial and then to a second order polynomial. In this

thesis, solutions were found via graphing and compared to results in simulation. A close match between theory and simulation was observed.

The first method also compared computed values of I^2t with simulation. Most were found to be within a five percent margin of error, mostly underestimates, which is preferable. These computed values were then put to the test with a physical experiment involving a Buck Converter, control and a ten ohm load. Fuses with known I^2t values were tested and the results mostly validate the theory presented in the first model. Conclusive evidence regarding the validity of this theory will require many more trial experiments with parameter value ranging over a wider set of values. In addition, other converters with current limiting control should be tested to determine that the theory is correct and independent of the hardware. Future work is also needed to empirically validate the second formulation.

Appendix A

Simscape™ model of Buck converter:

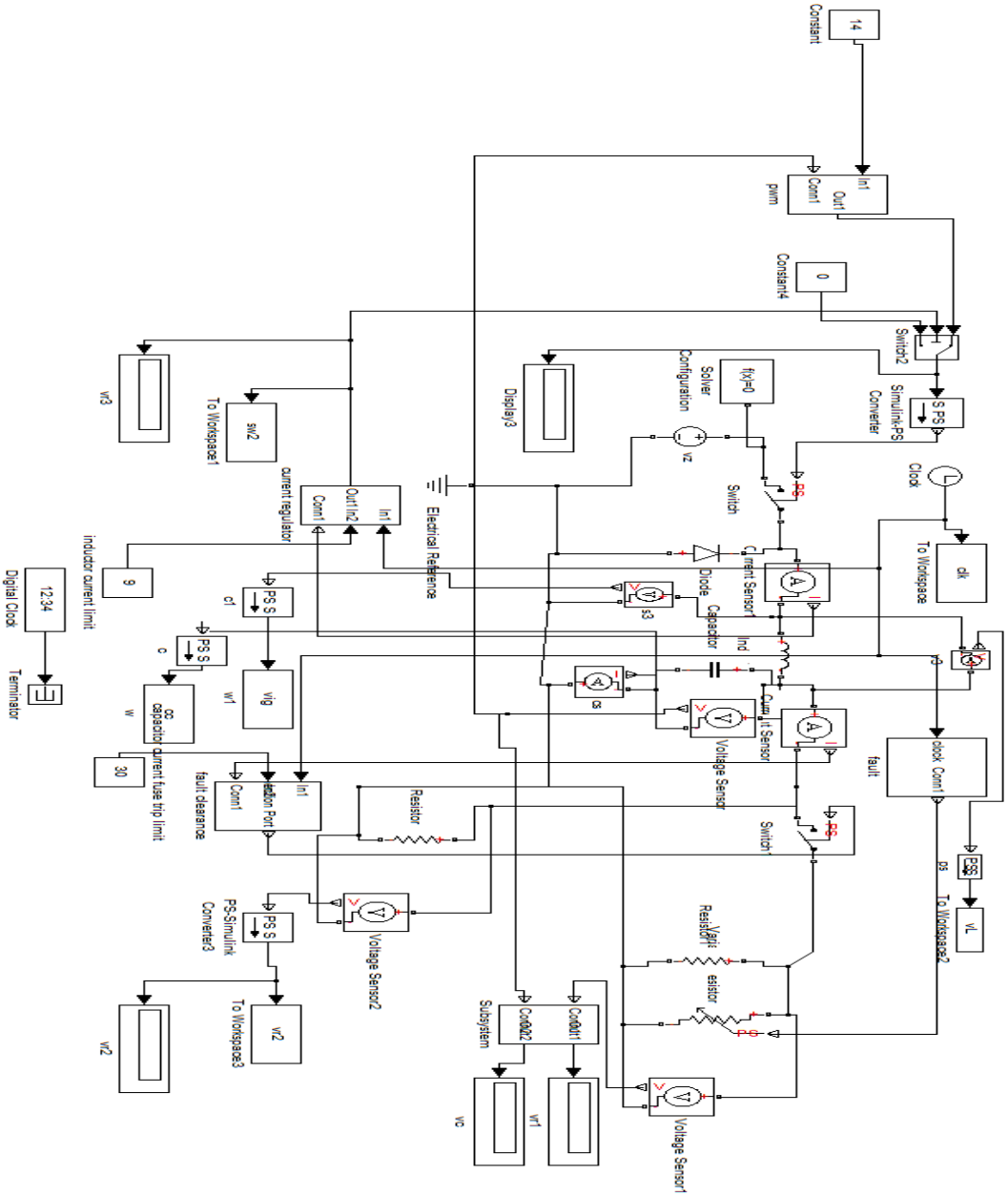

Fault Clearance

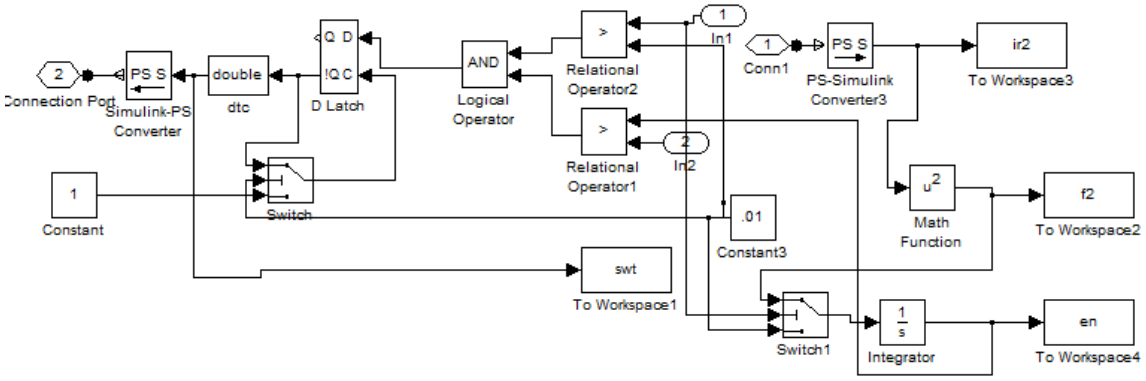

Fault control:

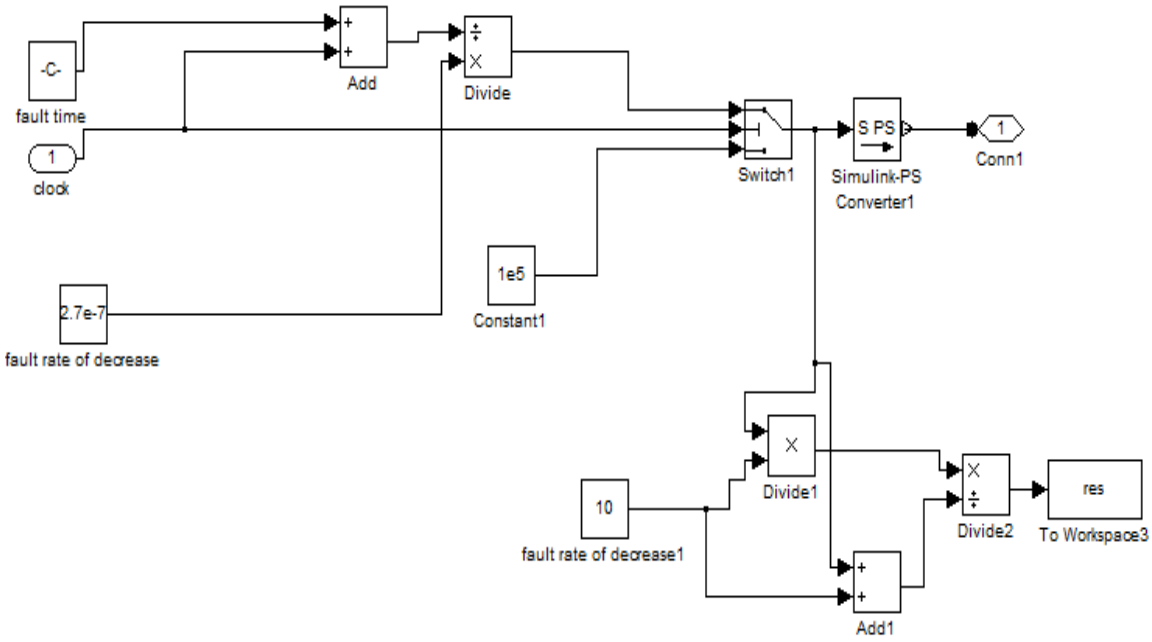

Duty Cycle Control:

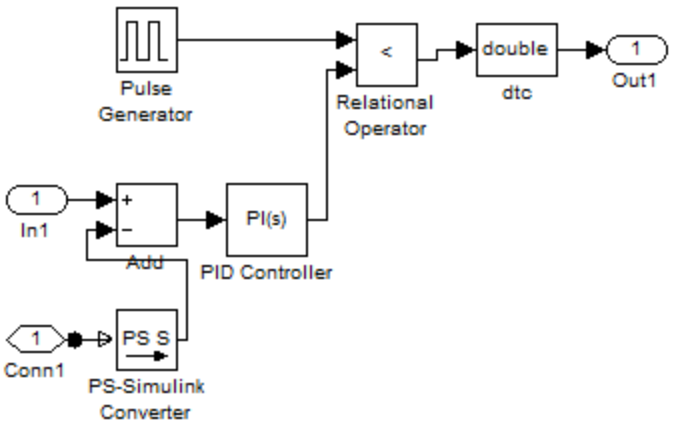

Current Limitation:

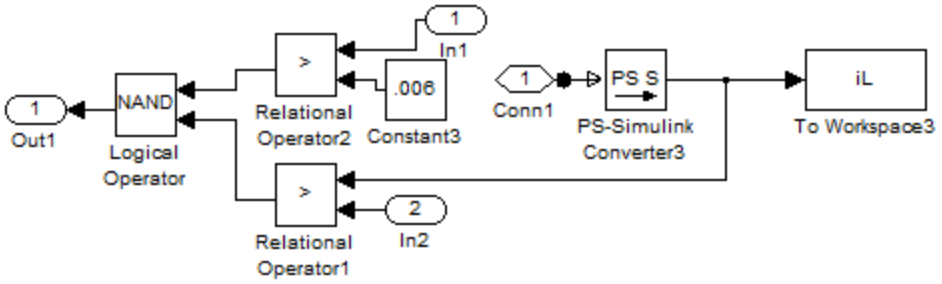

Alternative SimScape model:

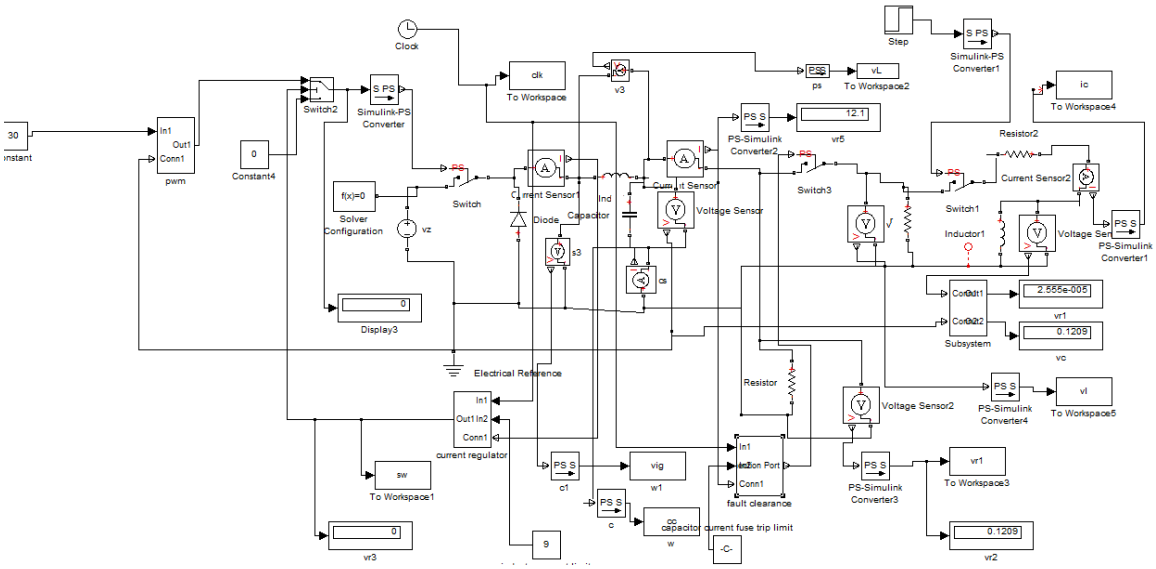

Appendix B

Equivalent Resistance Model Verification

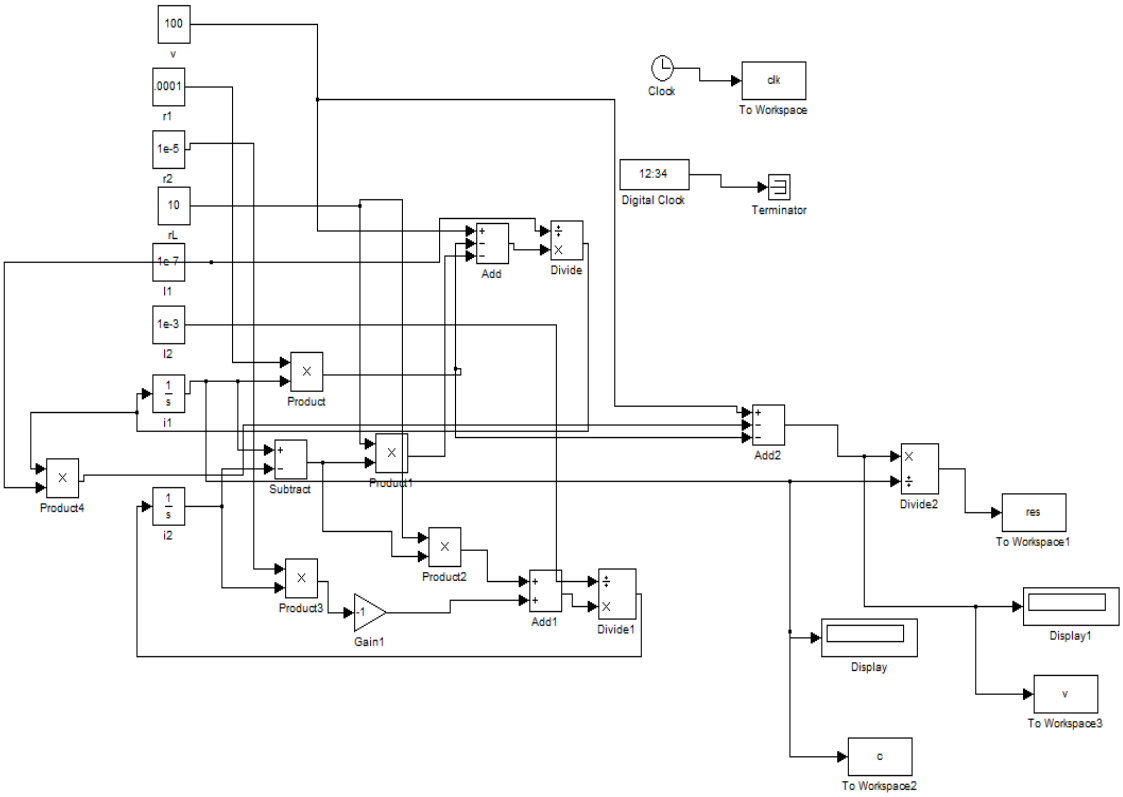

Appendix C

Fuse data sheet from Mouser Electronics.

Rated Current [A]	Rated Voltage [VAC]	Breaking Capacity	Voltage Drop 1.0 In max. [mV]	Voltage Drop 1.0 In typ. [mV]	Power Dissipation 1.5 I_n max. [mW]	Melting I^2t 10.0 In typ. [A^2s]	VDE	cULus	CCC	S	L	T	Order Number
0.04	250	1)	-	400	-	0.00016		●		●	●		0034.6000
0.05	250	1)	850	460	110	0.0004	●	●	●		●		0034.6001
0.063	250	1)	750	330	120	0.001	●	●	●		●		0034.6002
0.08	250	1)	650	280	140	0.001	●	●	●		●		0034.6003
0.1	250	1)	600	300	160	0.002	●	●	●		●		0034.6004
0.125	250	1)	550	210	180	0.006	●	●	●		●		0034.6005
0.16	250	1)	500	460	210	0.014	●	●	●		●		0034.6006
0.2	250	1)	480	470	250	0.024	●	●	●		●		0034.6007
0.25	250	1)	440	360	290	0.058	●	●	●		●		0034.6008
0.315	250	1)	400	345	330	0.104	●	●	●		●		0034.6009
0.4	250	1)	370	80	390	0.044	●	●	●		●		0034.6010
0.5	250	1)	350	75	460	0.09	●	●	●		●		0034.6011
0.63	250	1)	320	70	530	0.15	●	●	●		●		0034.6012
0.8	250	1)	300	70	630	0.22	●	●	●		●		0034.6013
1	250	1)	280	70	740	0.33	●	●	●		●		0034.6014
1.25	250	1)	280	65	920	0.68	●	●	●		●		0034.6015
1.6	250	1)	250	70	1000	0.94	●	●	●		●		0034.6016
2	250	1)	240	70	1360	1.3	●	●	●		●		0034.6017
2.5	250	1)	200	65	1310	1.9	●	●	●		●		0034.6018
3.15	250	1)	180	65	1490	5.4	●	●	●		●		0034.6019
4	250	2)	160	60	1680	7.9		●		●	●		0034.6020
5	250	2)	150	60	1970	11.2		●		●	●		0034.6021

Appendix D

MATLAB® code for computation of fault current:

```
format long

a=1e-6;
b=.09;
n=1;
ilm=9;
rt=.1;

sck=size(clk);

L=a;%6.00E-04%  1.00E-03    %2.00E-03%  3.00E-03    6.00E-03;
n=1;
%for c=1e-4:1e-5:2e-3;
c=3e-3;
r1=10;

a1=1/2/a/c;
a2=1/c/r1;
ils=1.3;

t=.09:rt/sck(1):rt;
sizt=size(t);
tp=t-b;
t0=4.22e-10*exp(-
1816577.97965541*L^2+4899.62979024404*L)/c^(124.7669*L+.97014);
t0=1.25e-8;

integK=ils/c/r1/a/2*sqrt(pi/a1)*exp(-
a2^2/a1/4)*erfz((sqrt(a1)*t0+a2/2/sqrt(a1))*j)./j;
K=ils/(r1*t0+a)*exp(a1*t0^2+a2*t0)-integK;

intQ=ilm/c/r1/a/2*sqrt(pi/a1)*exp(-
a2^2/a1/4)*erfz((sqrt(a1)*tp+a2/2/sqrt(a1))*j)./j;
%K=1.0160e8
ifault=(r1*tp+a).*exp(-(a1*tp.^2+a2*tp)).*(intQ+K);

if2=ifault.^2;
```

MATLAB® code for computation of I^2t values:

```
k=1;
while t(k)<.031
    k=k+1;
end

eq=sum(if2(1:k))*(t(k)-.03)/k

m=1;

while clk(m)<.03
    m=m+1;
end

n=1;


while clk(n)<.04
    n=n+1;
end

for k=1:n-m
    dclk(k)=clk(m+k)-clk(m+k-1);
end
sim=dot(f2(m:n-1),dclk)
%}
```

MATLAB® code for satisfying equation (3.2)

```
while max(ir2)<max(ifault)
   t0=t0+.00000001;
   integK=ils/c/r1/a/2*sqrt(pi/a1)*exp(-
a2^2/a1/4)*erfz((sqrt(a1)*t0+a2/2/sqrt(a1))*j)./j;
K=ilm/(r1*t0+a)*exp(a1*t0^2+a2*t0)-integK;

intQ=ils/c/r1/a/2*sqrt(pi/a1)*exp(-
a2^2/a1/4)*erfz((sqrt(a1)*tp+a2/2/sqrt(a1))*j)./j;
ifault=(r1*tp+a).*exp(-(a1*tp.^2+a2*tp)).*(intQ+K);
if2=ifault.^2;
max(if2)-max(f2)

end
```

Appendix E

Experimental Setup Photo:

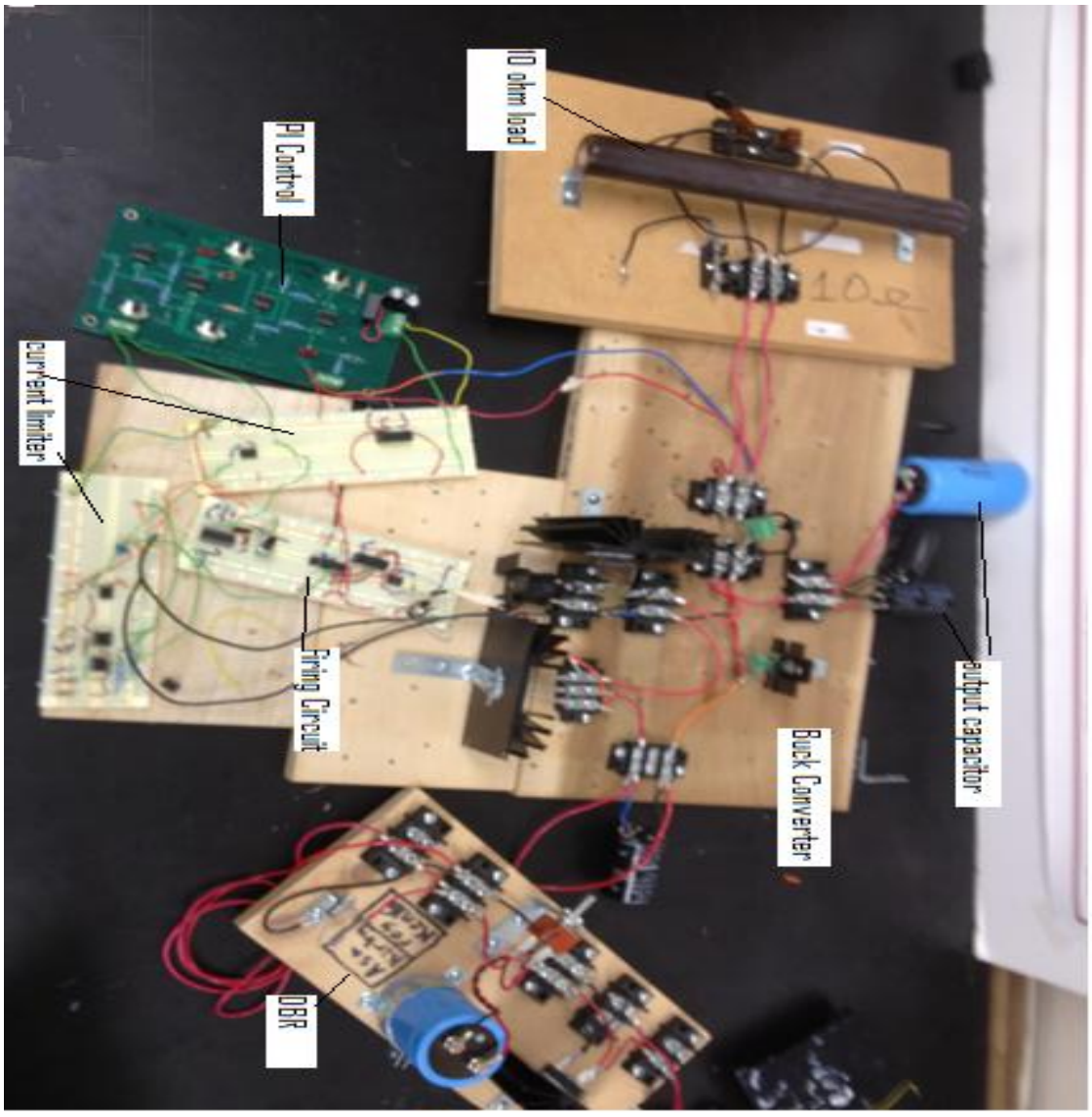

Bibliography

[1] Masters, Gilbert M. *Renewable and Efficient Electric Power Systems.* New Jersey: John Wiley & Sons, Inc., 2004. Print.

[2] S. Jeszenszky, "History of transformers", *IEEE Power Engineering Review*, Vol. 16, 1996, pp.9-12.

[3] D. Salomonsson, 2008, Modeling, Control and Protection of Low-Voltage DC Microgrids, Doctoral Thesis, Royal Institute of Technology, Stockholm, Sweden.

[4] Glover, J, Sarma, M, Overbye, T *Power System and Analysis Design 4th Eddition*. Stamford: Cengage Learning. 2008. Print.

[5] D. Meindl, ''A history of low power electronics: how it began and where it's headed'', *Proc. of Int. Symp. Low Power El. and Design*, pp. 149 -151, 1997.

[6] Melilo, A. McGuire, D. Kicklighter, B Moore III, C. Vorosmarty, A. Schloss. Global Climate Change and Terrestrial Net Production. *Nature*, 363, 20 May 1993,234-240.

[7] Anderegg, William R L; James W. Prall, Jacob Harold, and Stephen H. Schneider (2010). Expert Credibility in Climate Change, *Proc. Natl. Acad. Sci. USA 2010.*

[8] PB Weisz. Basic Choices and Constraints on Long-Term Energy Supplies, *Physics Today*, 2004.

[9] Murthy, M.S.; Patil, Y.S.; Sharma, S.V.K.; Polem, B.; Kolte, S.S.; Doji, N., Revolving Doors Producing Green Energy, 2011 *IEEE First Conference on Clean Energy and Technology*.

[10] A. Kwasinski, 2005, A Microgrid Architecture with Multiple-Input DC/DC Converters:

Applications, Reliability, System Operation and Control, Doctoral Thesis, University of Illinois at Urbana-Champagain.

[11] M. Saeedifard, M Graovac, R.F. Dias, R. Iravani, DC Power Systems: Challenges and Opportunities*, IEEE Power and Energy Society General Meeting*, 2010, 25-59 July 2010,1-7.

[12] T. C. Green and J. D. McDonald, "Modeling and analysis of fault behavior of inverter microgrids to aid future fault detection," in *Proc.IEEE Int. Conf. Syst. Eng.*, 2007, pp. 1–6.

[13] A. Kwasinski, Quantitative Evalution of DC Microgrids Availability: Effects of System Architecture and Converter Topology Design Choices, *Transactions on Power Electronics, IEEE*, Vol 26, Issue 3.

[14] Milo, A.; Gaztanaga, H.; Etxeberria-Otadui, I.; Bilbao, E.; Rodriguez, P. Optimization of an experimental hybrid microgrid operation: Reliability and Economic Issues, PowerTeck 2009 *IEEE Bucharest*, 1-6.

[15] Poh Chiang Loh; Blaabjerg, F, Autonomous operation of hybrid microgrid with AC and DC sub-grids, Power Electronics and Applications (EPE 2011), *Proceedings of the 2011-14th European Conference on, Publication Year*: 2011 , Page(s): 1 – 10.

[16] X. Liu, P. Wang, P. C. Loh, "A Hybrid AC/DC Microgrid and Its Coordination Control," *IEEE Trans. Smart Grid*, accepted for publication, 2011.

[17] Z. Jiang, X. Yu, "Hybrid dc- and ac-linked microgrids: Towards integration of distributed energy resources," *IEEE Energy 2030 Conference*, 2008.

[18] T. Panigrahi, A. Saha, S. Chowdhury, S. P. Chowdhury,N. Chakraborty, Y. Song, and S. Byabortta, "A simulink based microgrid modelling and operational analysis using distributed generators," in *International Universities Power Engineering Conference*,

Sep. 2006, pp. 222–226.

[19] T.Robbins, "Fuse model for over-current protection simulation of DC distribution systems", in *Proceedings of the Conference INTELEC*, 1993, pp.336-340.

[20] Chunlian, R. Dougal, and L. Shengyi, "Solid-state Over-current Protection for Industrial DC Distribution Systems," in *4th International Energy Conversion Engineering Conference and Exhibit (IECEC)*, June 2006.

[21] E. Sortomme, G. J. Mapes, B. A. Foster, and S. S. Venkata, "Fault analysis and protection of a microgrid," in *Proc. North Amer. Power Symp*., 2008, Sep. 2008, pp. 1–6.

[22] H. J. Laaksonen, "Protection Principles for Future Microgrids," *IEEE Transactions on Power Electronics*, vol. 25, pp. 2910-2918, 2010.

[23] Salomonsson, D.; Soder, L.; Sannino, A.; , "Protection of Low-Voltage DC Microgrids," *Power Delivery, IEEE Transactions on* , vol.24, no.3, pp.1045-1053, July 2009.

[24] B. Devearajan, Modeling of DC fuse for protection of semiconductor devices using PSCAD/EMTDC, University of Texas, Master's Thesis, 2010.

[25] J.A. Giancaterino, DC-DC converter plants and their ability to clear distribution fuses, *Telecommunications Energy Conference, , INTELEC '94*., 16th International 30 Oct 3 Nov 1994.

[26] M. Brucoli, T. C. Green, and J. D. F. McDonald, "Modelling and analysisof fault behaviour of inverter microgrids to aid future fault detection," *IEEE International Conference on System of Systems Engineering*, pp. 1-6, 2007.

[27] Yujie Zhang, Jimena Bastos, Noel N. Schulz And Daxa Patel, "Modeling and Testing of Protection Devices for SPS using MATLAB/Simulink and VTB," *Proceedings Of The IEEE Electric Ship Technologies Sympoisum (ESTS 07)*, Arlington, Virginia, May 2007.

[28] Este, H.B, Kwasinski, A; Hebner, R.E., Uriarte, F.M.; Gattozzi, A.L.;, "Open Series Fault Comparison in AC & DC Micro-grid Architectures" *Telecommunications Energy Conference (INTELEC)*, 2011 IEEE 33rd International, pp1-6.

[29] Kaufmann, R.H,; "The Magic of I2t"; *IEEE Transaction on Industry and General Applications*; vol. IGA-2 No. 5; Sep./Oct. 1966.

[30] Grashtein, I.S, Table of Integrals, Series and Products, Amsterdam, Boston: Academic Press, 2007, 7th Edition.